OTTO VON GUERICKE UNIVERSITÄT MAGDEBURG

FACULTY OF COMPUTER SCIENCE

Communication and Networked Systems

Communication and Networked Systems

Bachelor Thesis

3D Scan Applications in Logistics: Using CoAP with RGB-D Cameras

Fabian Hüßler

Supervisor:	Prof. Dr. rer. nat. Mesut Güneş
Assisting Supervisor:	MSc. Marian Buschsieweke

Institute for Intelligent Cooperating Systems, Otto-von-Guericke-University Magdeburg

August 6, 2020

Abstract

Abstract

The embedded devices which form the Internet of Things (IoT) experience a rapid development in increasing processing power and decreasing chip sizes and prices. Future homes will be equipped with smart network interoperable devices, which will communicate over various network protocol stacks. In the fields of home- and industrial automation, cameras providing color and depth information prove to be very useful in many applications such as face recognition, pose tracking or environmental 3D scanning.

The Constraint Application Protocol (CoAP) is a popular IoT protocol for low power and lossy wireless networks. CoAP is commonly used to transmit small sized sensor data, while image sizes may be in the order of MB. This thesis aims to provide a comprehensive Application Programming Inteface (API) to make camera resources from the state of the arts low cost Intel RealSense RGB-D (color and depth) cameras retrievable for a CoAP client. It also gives an insight in basic camera concepts and the use of cameras for logistic companies. As an example, the provided CoAP client computes the object dimensions of received point cloud data and may show the color image and the depth image in grayscale values. The client may monitor a resource, while it repeats the initial request. The application is tested in several test cases, which show that CoAP can be used for simple 3D scan applications, but packet drops become a bottleneck because with default protocol parameters (`NSTART = 1`), CoAP effectively becomes a “stop and wait” protocol. The median to transmit a color image with a resolution of 1280x720 pixels over a wireless network is 14.6 s. The median to transmit a full point cloud from a depth image with 1280x720 pixels over a wireless network could be reduced to 16 s.

Contents

List of Figures

List of Tables

Listings

Acronyms

API Application Programming Inteface. iii, 2, 7, 9, 10, 20, 43

ASCII American Standard Code for Information Interchange. 12

CoAP Constraint Application Protocol. iii, 1–3, 5, 7–11, 14, 15, 18, 23–26, 43, 44

DTLS Datagram Transport Layer Security. 1, 2, 10

FPS Frames per Seconds. 12, 16, 17

FRD Fully Distributed Resource Discovery. 5

HTTP Hyper Text Transfer Protocol. 1, 2, 5

ICP Iterative Closest Point. 14, 17

IMU Inertial Measurement Unit. 11

IoT Internet of Things. iii, 1, 5, 7

JSON JavaScript Object Notation. 11, 16–18, 21

MQTT Message Queuing Telemetry Transport. 1–3, 8, 43

MQTT-SN MQTT for Sensor Networks. 1, 2

MTU Maximum Transmission Unit. 5

NTP Network Time Protocol. 8

PRD Proactive Resource Discovery. 5

REST Representational State Transfer. 1

SLAM Simultaneous Localization and Mapping. 5

SVD Single Value Decomposition. 14

TCP Transmission Control Protocol. 2, 43

UDP User Datagram Protocol. 1, 2, 8

URI Unified Resource Identification. 1, 2, 10, 12, 16

Glossary

E-Commerce Commerce over the Internet. 1

Extrinsic Parameters Rotation matrix and translation vector. 21

Focal Length Distance from the Principal Point to the camera sensor. 20

Industry 4.0 4th industrial revolution - Automated customizable and self-regulated manufacturing processes with the help of IT and networked systems. 1

Intrinsic Parameters Camera specific values - Focal Length Principal Point Lense Distortion and Distortion Model. 20

Principal Point Point on the image plane onto which the perspective center is projected. 20

RealSense RGB-D camera series from Intel. iii, 2, 6, 7, 9, 11, 16–18, 20, 21, 23, 26, 43

RGB-D Camera that provides color (RGB) and depth (D) information with each pixel.. iii, 1–3, 5, 7, 43

CHAPTER 1

Introduction

There are more devices connected to the IoT than people living on earth and prognosis predict that by 2025 it will be more than 75 billions [1]. Cameras are an essential part of Industry 4.0 and the world of smart devices. Sensors to capture visual information equip robots with the most important sense of humans, the sight. While industrial laser scanners are a costly purchase, modern depth cameras may offer an acceptable alternative [2]. With the gain of image information from color and depth images, machines are able to complete complex tasks, e.g. estimating the load status of a truck or 3D reconstruction.

Industry 4.0 is significantly driven by the IoT [3] and thus takes advantage of network protocols for constraint devices, such as Message Queuing Telemetry Transport (MQTT) [4], CoAP [5] or MQTT for Sensor Networks (MQTT-SN) [6] to meet the demands of constraint devices with limited memory and processing power. When it comes to large payloads beyond the size of simple temperature and humidity data, further challenges appear like the negotiation of block sizes in a network of heterogenous devices, packet loss and latency.

With the success of E-Commerce, logistic companies like DHL or UPS have to deal with a continuous growth of packet deliveries [7]. Prices are often calculated by package weight and size. Hence, logistic companies profit from an automatic and reliable estimation of packet and load sizes in their workflow. Packets usually have a barcode or a QR code attached that must be scanned to coordinate the delivery process. RGB-D sensors may serve both purposes. The distribution of RGB-D data from a camera in a constraint network requires an appropriate network protocol.

CoAP is a popular IoT protocol which has originally been proposed by Shelby et al. in RFC 7252 [5]. CoAP runs over User Datagram Protocol (UDP) and has been designed to make resources in constraint networks easily accessible through the web. CoAP is closely related to Hyper Text Transfer Protocol (HTTP) [8], as they share common request methods and response codes. CoAP and HTTP are conform to the Representational State Transfer (REST) [9] architecture. Resources are uniquely identifiable by their Unified Resource Identification (URI) [10] and each request must be processed independently by the server. Communication over CoAP can also be secured by a Datagram Transport Layer Security (DTLS) layer. Similar to the `https://` scheme, there exists the DTLS secured `coaps://` scheme. Due to the unreliable message delivery of UDP, CoAP introduces the possibility to initiate a reliable communication as indicated by the message type. Reliable messages are marked as confirmable and become retransmitted with an exponential backoff until a matching acknowledgement is received or the number of maximum retransmissions would be exceeded. Unlike CoAP, MQTT runs over Transmission Control Protocol (TCP), thus it already guarantees that messages arrive in order and reliable. The MQTT protocol may seem to be the better choice if large payloads must be transmitted. This thesis investigates if CoAP could be used with RGB-D cameras. Specifically a resource API is presented that provides a RESTful interface to the Intel RealSense D400 cameras.

1.1 Motivation

While MQTT has prevailed for many companies, the use of CoAP is motivated by convenience, rather than performance. The most convenient user interface probably is a web browser, as almost everyone uses it daily with mobile or stationary devices and is able to operate it. For employees in a logistics center or for any kind of customer, it would be easy to retrieve sensor information over a web browser. To build a bridge between web browsers and CoAP endpoints with camera interface, HTTP-CoAP and CoAP-HTTP proxies could map messages between both protocols. The mapping between CoAP and HTTP is best explained in RFC8075 [11]. CoAP may be a choice to transmit camera data in a live stream because it runs over UDP. Therefore, cameras could be used for monitoring.

The CoAP multicast feature is an easy solution to aggregate camera data if cameras are distributed across multiple endpoints. In practice, multiple cameras are often used for 3D reconstruction [12] or if the scan area cannot be covered by the field of view of only one camera. Endpoints in constraint networks are more affected by failure rates. If cameras are distributed over multiple endpoints, services could be held up at least partially or another camera could be calibrated to substitute the failed endpoint. Processing also becomes more balanced when one endpoint does not have to serve requests for more than one camera. Although it is not trivial to map a HTTP request to a CoAP multicast request and wait for multiple responses because HTTP lacks multicast support, it is mentioned in RFC8075 [11]. CoAP group communication is well defined in RFC7390 [13].

CoAP integrates a resource discovery mechanism that makes it easy for clients to discover new cameras. The resource discovery can be used in combination with multicast to get all resources from multiple endpoint with a single request. Clients may further limit the response payload size while they filter by the desired type of resource. For example to filter by group resources, a client appends `rt=core.gp` to the URI query in a discovery request. A resource directory [14] is a further resource discovery improvement in a network with many nodes and many resources. The resource directory is a central point where nodes are supposed to register their resources and update them periodically.

Comparisons with MQTT-SN have shown that CoAP needs more time to complete a regularly scheduled single hop transmission and that messages arrive less reliable in a multi hop scenario but energy consumption is lower [15]. In the scenario presented in [16], MQTT-SN had a 30% better average transmission time than CoAP. Another publication showed that CoAP may outperform MQTT when the packet loss rate is greater or equal to 25%. The message overhead generated with CoAP is smaller than that of MQTT, as long as payload sizes do not exceed about 320 B [17].

1.2 Thesis Structure

The remaining of this thesis is structured as follows.

The next section puts this thesis into a context of existing work. Chapter 3 first gives an overview of the application in Section 3.1 that is contributed with this thesis. Then Section 3.2 shows the application- and CoAP resource architecture. Section 3.3 states how the resource semantics have been implemented and what they do exactly. After that, Section 3.3.5 tells what image processing is done to complete the application task. This thesis includes experiments in Section 3.4 that test the performance of the application. Following, experiments are evaluated in Section 4.1. Finally, a conclusion will be drawn in Section 5.1 if CoAP could be used to transmit RGB-D camera data in logistic application fields.

CHAPTER 2

Related Work

Since the proposal of CoAP in 2014, a lot of extending work has been put into it. Some common and important extensions are the block-wise transfer [18] to make it possible to transmit large payloads that exceed the Maximum Transmission Unit (MTU) of CoAP, without IP fragmentation, and the OBSERVE option [19] that extends CoAP with a push mechanism, based on client subscriptions. Further research was done to facilitate CoAP group communication [13] and guidelines to map between HTTP and CoAP were proposed [11]. A lot of research was done to ease resource discovery. There are centralized Proactive Resource Discovery (PRD) [20] solutions with a resource directory and there are Fully Distributed Resource Discovery (FRD) [21] approaches. In PRD, the resource directory sends advertisements so that new nodes may become aware of it very quickly. In FRD, resource descriptions are propagated by a flooding algorithm. CoAP has become very popular in the IoT, hence there are a lot of implementations in different languages. A performance analysis of several CoAP implementations has been conducted by Marker Iglesias-Urkia et al. [22]. Their tests showed that *libcoap* is one of the fastest libraries.

Companies with focus on industrial automation are using RGB-D cameras to develop new applications for their customers in the logistics sector. For example, Thorsis Technologies in collaboration with the Fraunhofer institution in Magdeburg have developed a framework for different RGB-D cameras [23]. It provides different applications, like simple package scan, scan of euro pallets and load supervision in a truck.

In robotics, RGB-D cameras are frequently used to perform Simultaneous Localization and Mapping (SLAM). The robot's task in SLAM is to construct a 3D map of it's environment and capture the path on which it was moving. Endres et al. [24] presented one of the first RGB-D SLAM systems, where the only sensor has been a Microsoft Kinect v1.

There are different approaches how cameras calculate depth values. An early technique was structured light [25]. Structured light imposes that an irregular but known infrared pattern is traced into the scene and an infrared camera observes the projected pattern. Depth values are triangulated from the disparity of the known pattern and the projected pattern. While the Microsoft Kinect v1 works with structured light, Kinect v2 measures the Time-of-Flight [26] for a laser that is traced into the scene and reflected back to the camera. A comparison of Kinect v1 and Kinect v2 has been done by Wasenmüller et al. [27].

They concluded that the Kinect v2 delivers more accurate depth values, even across longer distances but is more affected by temperature than the Kinect v1 camera. They have also noted that multiple structured light cameras interfere each other. The cameras used for this thesis are Intel's RealSense D400 [28] depth cameras, which compute depth information from stereo vision [29]. For stereo vision, two cameras must produce rectified images of the same scene which means that a pixel in one image must correspond to a pixel in the other image, where the corresponding pixel is only shifted in horizontal direction. Finding corresponding pixels can be hard in textureless scenes, thus Intel's cameras also include an infrared projector [30] to produce an artificial texture. Carfagni et al. [31] have compared the model D415 with Intel's previous generation of depth cameras, with regards to short rage depth quality. They found the D415 to be more precise. Intel has published a collection of papers, regarding their D400 camera series. These papers include methods for camera fine tuning [32], power over Ethernet [33], image post processing [34], the use of multiple cameras [35], an explanation of the infrared projectors [30] and a guide to perform a camera calibration [36].

CHAPTER 3

Thesis Contribution

This chapter presents the results that could be achieved with the work on this thesis. Firstly, the implementation scope is given in Section 3.1. Following, the application architecture is described and the structure of the CoAP resource API is presented in Section 3.2. As a main part, Section 3.3 shows implementation details of the utilized CoAP library and the camera interface and explains CoAP resource semantics. It also puts a focus on image processing. Finally, 11 experimental test cases are introduced in Section 3.4 to show the influence of image resolution, network and post processing on the application performance.

3.1 Application Scope

The application presented in this thesis is an example that shows that CoAP can serve as an appropriate and lightweight communication protocol for basic scan applications as they can be found in today's logistic companies [37]. CoAP has been designed to work in networks consisting of constraint IoT devices, hence large payloads are not typical and the CoAP block-wise transfer [18] extension becomes a necessary implementation requirement to transmit images and point cloud data considering that high resolution images of 1280 $\times$ 720 pixels in RGB format have an uncompressed size of 2.7648 MB. Similar a point cloud obtained from a depth sensor running at a low resolution of 640 $\times$ 480 pixels has an upper bound of 307 200 points. On the assumption that each point is represented as 3 floating point values, where each float has a size of 4 B, the size of that point cloud is at most 3.6864 MB. With the provided application a CoAP client is able to access the camera's color, depth and point cloud resource for general purpose image processing. The point cloud data can be retrieved unfiltered or the client can set dimension upper and lower bounds and post processing options to reduce the number of points in a response in order to limit transmission sizes. As an example, the client is able to compute the minimal box shaped packaging for any object that can be captured with one or multiple cameras that can be run on the same or separate endpoints. The application does not provide a framework for any RGB-D sensor but has been developed to work with the D400 series of the Intel RealSense sensor family. The single-sensor application builds the basis for the multi-sensor application and thus is the simpler one. More than one sensor might be required to create a 3D reconstruction of a scene. That can be done with multiple sensors which are either oriented inwards, e.g. to reconstruct a human, or oriented outwards, e.g. to reconstruct a room. The latter cannot be done with this application because there won't be a common point for cameras that are oriented in opposite directions. The first kind of reconstruction could be done with this application, as one might have one camera for the front, back, left and right sight of an object. The 3D reconstruction shall not be the task for the presented application. Instead, the task will be to find the object's x-, y- and z-dimensions which form a minimal packaging box with one and multiple sensors. Sometimes even that could require multiple sensors if the object is too large. A prior configuration step must be done before the points obtained from multiple cameras can be processed together. Because each camera defines their points relative to it's own position as the origin $(0, 0, 0)$. The points of each camera must be transformed into a common coordinate system [38]. For that purpose a separate tool is provided with this thesis. The 3D-Transformation tool determines the transformation parameters, rotation matrix and translation vector, and visualizes the transformed point cloud of one or more sensors. The user is able to perform manual correction if needed. The tool can also be compiled for embedded hardware without additional visualization. Another difficulty when a task is carried out by multiple sensors is that sensors can be distributed across several devices. In the particular case of multiple cameras there must be a way to trigger all nodes to capture a new image at the same time. Due to the UDP transport protocol, CoAP is already capable to trigger multiple endpoints by simply sending an IP multicast scan request. However, this may not result in fully synchronized images since each camera may still grab their new image at slightly different times depending on request arrival time and the delay it takes to grab an image. The current implementation makes use of the CoAP multicast feature but does not perform any time synchronizing mechanism. Such a mechanism could be a high resolution timestamp, e.g. in milliseconds that is provided with every image. Besides that, all endpoints must be configured to have a common timer. In a secure network the Network Time Protocol (NTP) [39] could be used to synchronize the system clocks of all sensor nodes in periodic time intervals. Considering security issues, NTP might not be an appropriate solution because an attacker could fake it's source IP address and would cause another client to be swamped with NTP responses to the monlist command [40]. Even the synchronization of multiple cameras connected to a single device can be a problem. For that purpose, Intel integrated a sync-cable port into their D400 camera series [35]. The synchronization can be achieved either by one camera acting as the master and the others acting as slaves or the slaves can be triggered by an external signal.

3.2 Architecture

The application consists of a CoAP server and a client implementation. Server and client exchange messages according to the request-response model, where the communication is always initiated by a client that sends a request to the server which sends an appropriate response. This approach has been chosen because this is the default CoAP message exchange method. In contrast to the request-response model, the publish-subscribe model as implemented by the MQTT protocol also could have been implemented with the CoAP `OBSERVE` option, that can be present in a `GET` request. In a scenario where data needs to be transmitted regularly, e.g. for live streaming, this would be the preferred approach since it omits a regular request being send and thus reduces network bandwidth consumption.

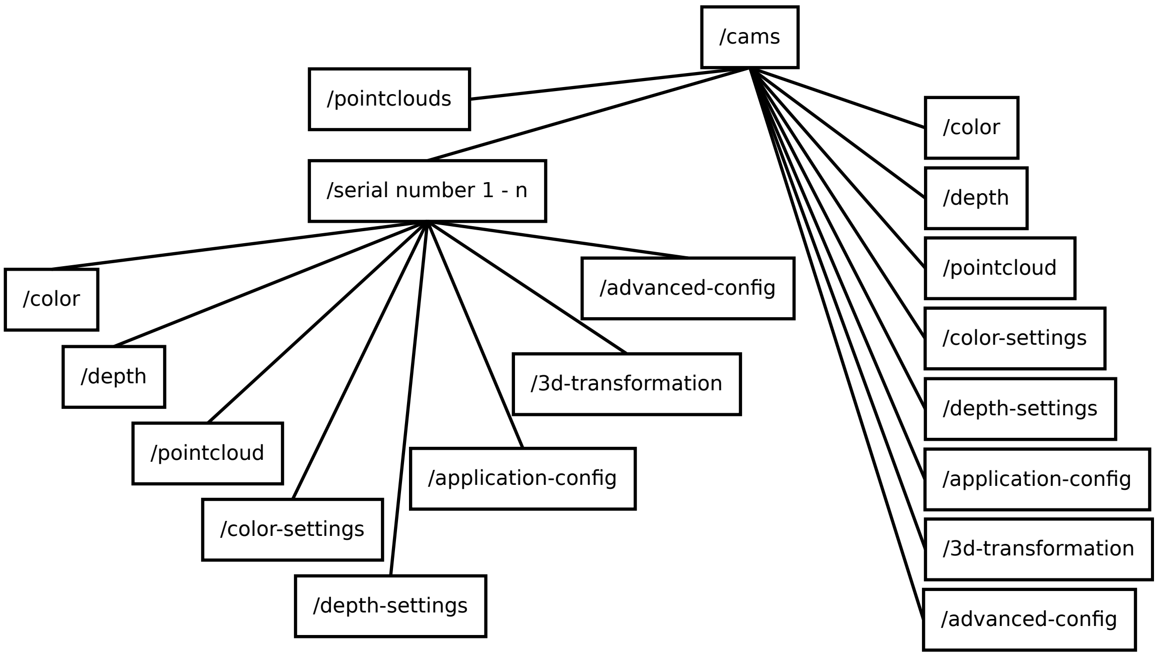

Figure 3.1: Application resource tree

Thanks to the modularity of the `OBSERVE` option, this feature could be added at any time which makes CoAP fit a wider range of application scenarios. The server's task is to provide a camera- and application configuration interface and to provide CoAP resources to retrieve the relevant camera data which are color and depth image data and point cloud data. For that it utilizes the camera specific API. The client's tasks are to configure the cameras with application dependent parameters and to perform the image processing. For each connected camera the server provides an individual configuration API in the form of CoAP resources. The sensors of an Intel RealSense camera, i.e. color and depth sensor, are working independently of each other. Thus both sensors are configured independently as well. The server also holds persistent resources to create the configuration and data retrieval resources. Color and depth images are retrieved from each camera separately and point cloud data can be retrieved either by addressing a specific camera path segment or by the general point cloud path segment. The general point cloud resource initiates a depth image grab for all connected cameras and the server returns their computed point clouds. For that reason all cameras of an endpoint should be provided with appropriate transformation parameters so the server can transform all points into a common coordinate system. This is explained in Subsection 3.3.4. Figure 3.1 shows all application resources as a tree and Table 3.1 shows their applicable request methods.

3.3 Implementation

In this section, the implementation details are going to be elucidated. On the one side the CoAP library and CoAP resources are presented in Subsection 3.3.1 and on the other side

URI Path	GET	POST	PUT	DELETE
/cams	no	no	no	no
/cams/pointclouds	no	yes	no	no
/cams/color	no	yes	no	no
/cams/depth	no	yes	no	no
/cams/pointcloud	no	yes	no	no
/cams/color-settings	no	yes	no	no
/cams/depth-settings	no	yes	no	no
/cams/application-config	no	yes	no	no
/cams/3d-transformation	no	yes	no	no
/cams/advanced-config	no	yes	no	no
/cams/<serial nr.>/color	no	yes	no	yes
/cams/<serial nr.>/depth	no	yes	no	yes
/cams/<serial nr.>/pointcloud	no	yes	no	yes
/cams/<serial nr.>/color-settings	yes	no	yes	yes
/cams/<serial nr.>/depth-settings	yes	no	yes	yes
/cams/<serial nr.>/application-config	yes	no	yes	yes
/cams/<serial nr.>/3d-transformation	yes	no	yes	yes
/cams/<serial nr.>/advanced-config	yes	no	yes	yes

Table 3.1: Allowed Application Resource Methods

the image processing in Subsection 3.3.5 and the camera API in Subsection 3.3.2 are in focus.

3.3.1 The CoAP Library

The used CoAP library for this project is an own implementation in C and does not support the entire RFC7252. The current implementation does not provide a DTLS layer to handle secure communication over the *coaps://* scheme. Furthermore the library does not support proxying. In order to satisfy the application requirements the CoAP block-wise transfer as of RFC7959 and CoAP group communication as proposed in RFC7390 are implemented in a simplified manner. The server side has to create CoAP resources. The user must provide the URI path, the content format and CoRE Link Format [41] attributes which are returned in a resource discovery response to the dedicated resource at `.well-known/core`. Optionally the user can provide a pointer to an Etag variable that the user must keep updated. The library examines this variable to issue a `2.03 VALID` response and for the if-match option. If the resource size is known in advance the user can provide an allocated buffer and must provide the buffer size and the size of the resource. These information become attached to the CoAP resource handle. To handle the request methods `GET`, `POST`, `PUT` and `DELETE` the user must provide function callbacks and a pointer to some optional user data that shall be passed as a callback argument. When the resource has been successfully created the user calls the register function in which ownership of the resource handle is passed to the library. Internally registered resources are organized in a list which is sorted by the resource URI path. When a client sends a request that matches a registered resource the appropriate method callback is called with a general library handle argument which is called `coap_interaction`, the received CoAP message, a convenient struct that holds pointers to all present request options and the user created resource handle along with the generic user data. Within the method callback the user should send the response according to the CoAP request/response semantics. If the user decides to respond to a confirmable message in a separate response he or she must send an empty acknowledgement and any time later he or she can send the response. For example the user could use a thread that waits for the resource to become ready and as soon as that becomes true, the server sends the response. The client side must first create a `coap_interaction` handle to send a request. To that handle the user can attach a response callback together with some general user data which shall be passed as a callback argument. The response callback also receives a struct holding pointers to present options in the response, the original request CoAP message and the response CoAP message. Within the response callback the client should copy the response payload to an appropriate location. Most importantly, the response callback is where the client sends the next payload block in case of a present BLOCK1 option in a `2.31 CONTINUE` response or requests the next payload block to be send in case of a present BLOCK2 option in a `2.05 CONTENT` response. The `coap_interaction` structure is the general library handle. In the sense of CoAP this handle represents the lifetime of a CoAP token that belongs to a CoAP remote node. Internally the interactions are stored in a hash table to achieve short response times. Not visible to the user, any `coap_interaction` has it's next timeout attached. The timeouts are organized in a future event list which is internally programmed as a heap data structure. The CoAP library provides `GET`, `POST`, `PUT` and `DELETE` resource handlers for the `coap-group` resources described in RFC7390 [13]. In RFC7390 the `application/coap-group+json` content format is proposed. The JavaScript Object Notation (JSON) content-format makes the CoAP library depend on a JSON library that has been chosen to be the cJSON library [42].

3.3.2 The Camera

The Intel D400 camera series [28] is the latest generation of Intel's RealSense depth and color sensors that have been released in January 2018. Since November 2018, the D435i has been released. It integrates an Inertial Measurement Unit (IMU) into the D435 camera to make the camera capable of estimating it's own pose which makes it well suited for robotics and tracking applications. The cameras must be run over USB 3.0 to fully exploit their capabilities, i.e. to enable all camera formats and resolutions. For this thesis two Intel RealSense D415 cameras have been tested. They are the cheapest model. The Intel D415 is best suited for 3D scan applications [31] because it has a smaller field of view than the D435 and D435i. It delivers the best depth results when running at a resolution of 1280x720 pixels [32]. Thus the same number of pixels covers a smaller area of the scene. Unlike the D435 and the D435i, the D415 has a rolling shutter rather than a global shutter. A rolling shutter does not work well for tracking applications where moving objects must be captured because the image exposure is done line or column wise and not all pixels at once. Thus distortions are the consequence.

Each D400 camera can be interfaced with the *librealsense* library [43] from Intel. Natively, the library is programmed in C++ but the developers provide various wrappers, for example for Python, Android and C. The low level C wrapper has been used to develop the present application. The easiest way to get started with the cameras is to use the high level *pipeline* class. The user just has to fill a *config* object with the stream resolutions, stream types, Frames per Seconds (FPS) and stream formats, pass it to the pipeline and the device starts streaming. The pipeline is able to output synchronized color and depth frames according to frame timestamps. The pipeline class has not been used for the current implementation because continuously streaming of depth and color data would decrease the performance on embedded systems and is not necessary to fulfill the application task. Instead, color and depth sensor open and close for each grab. For each packet kind there exists an application header that is uniquely identifiable by the *type* field to let a client process the received packet appropriately. The headers are depicted in Figure 3.2. The fields *Image Width* and *Image Height* are a 16 bit unsigned integer in network byte order and build the image resolution. For a point cloud packet, the *Number of Points* field is the number of points as a 16 bit unsigned integer in network byte order. The field *Pixel Size* and *Point Size* are the size of a pixel or a point in bytes, respectively. The *Timestamp* field is a 32 bit UNIX timestamp in network byte order. For a depth packet, the *Depth Scale* is a floating point number. The meaning of the depth scale is explained in Subsection 3.3.3.

3.3.3 Resource API

This subsection explains the application resource semantics and implementation details. Some resources only exist to create new resources as it is often the case for `POST`. Requests to retrieve, color, depth and point cloud data must use the `POST` method as well because they trigger a new grab, hence the resource changes and requests are not idempotent. Some resources must exist for each camera. Those are automatically created and deleted when a device becomes connected or disconnected, respectively. This has been implemented with the `rs2_set_devices_changed_callback()` function from *librealsense*. However, in case of an error, in some use cases it might not be the easiest way to just go to the device and replug it. In that case one could delete and recreate the device specific resources.

Resources to create camera specific resources

The resources to create the camera specific resources are depicted on the right side of Figure 3.1 and only support the `POST` method. A request to these resources must contain the serial number of the camera whose resource shall be created. The serial number is encoded in American Standard Code for Information Interchange (ASCII) characters and is expected to be 12 digits in length. In case that there is no camera with the specified serial number connected, a `4.00 BAD REQUEST` response is returned. The sequence diagram in Figure 3.3 shows the message flow of a successful resource creation of the color resource for a certain camera. The message flow is the same for all other resource creation resources, with respect to the URI. Thus it serves as a reference.

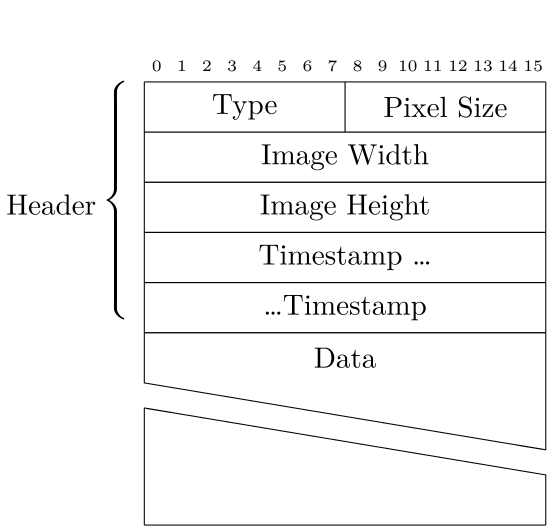

a) Application packet format for a color image packet

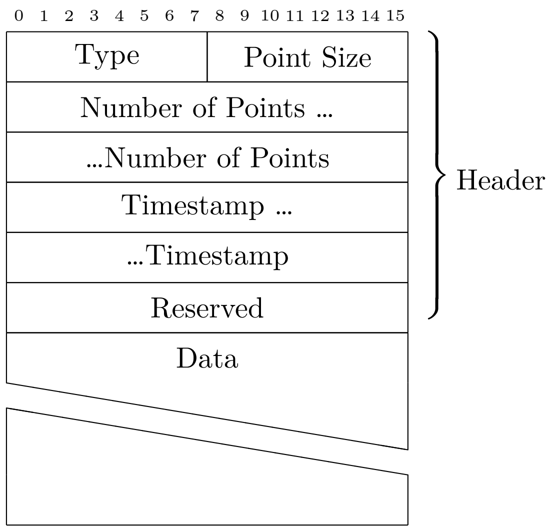

b) Application packet format for a point cloud packet

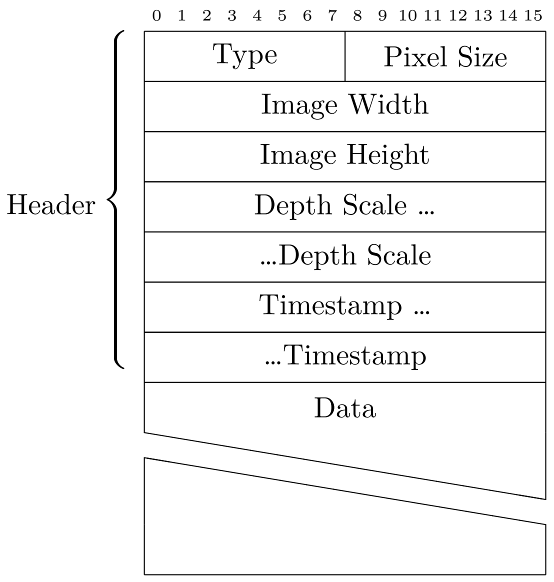

c) Application packet format for a depth packet

Figure 3.2: Packet field layout of color, depth and point cloud packets

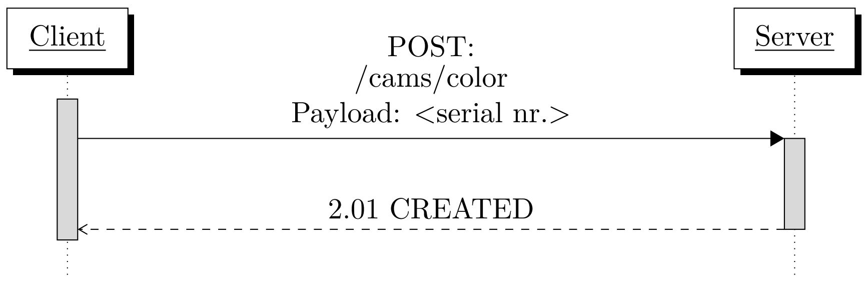

Figure 3.3: CoAP message flow of a successful resource creation of the color resource for a certain camera

Resource: /cams/pointclouds

When the server receives a `POST` request for the general point cloud resources it triggers a grab of a depth frame for each connected camera in a new thread. Then a point cloud is computed for each depth frame. That is performed by the *librealsense* library. The server processes the points according to previously set application and transformation parameters. It filters the points by a 3D region of interest, applies some of the *librealsense* post processing blocks and performs a 3D transformation, if transformation parameters have been set, which should have been done before because all points are put together in a single buffer. The server may perform an Iterative Closest Point (ICP) algorithm to register multiple point clouds. This has been implemented in the most simple way, using the Single Value Decomposition (SVD) approach [44]. The SVD is computed with *gsl* [45]. However, this introduces more computational overhead than it increases accuracy because of a brute force nearest neighbour computation. The parameters obtained from a 3D marker transformation, e.g. with *ArUco* [46] markers, have been found sufficiently accurate [35] for this application. The client does not know from how many cameras the points come from. If no camera was able to grab a new depth frame then the server only returns the header for a point cloud packet which has set the number of points field to zero. Upon success CoAP block-wise transfer with the `BLOCK2` option is involved. The message flow to receive all point clouds from all connected devices is shown in Figure 3.4. After that the usual block-wise transfer follows.

This resource can also be requested in a multicast request to retrieve all point clouds from all cameras, connected to all endpoints that have joined a certain multicast group. This allows the cameras to be distributed across multiple network endpoints. Again, all cameras in a group should be provided with transformation parameters to have a common origin. An endpoint may join a multicast group, if a `POST` request is sent to the dedicated `coap-group` resource. For example the `POST` request may contain the payload: `{"a":"224.0.0.121"}`, to make a server join the multicast group with the address `224.0.0.121`.

Resource: /cams/<serial nr.>/color

This resource is used to retrieve a new color frame from the camera with the serial number <serial nr.>. Only the `POST` method can be applied to this resource. Upon success CoAP block-wise transfer with the `BLOCK2` option is involved. Figure 3.5 shows the message flow

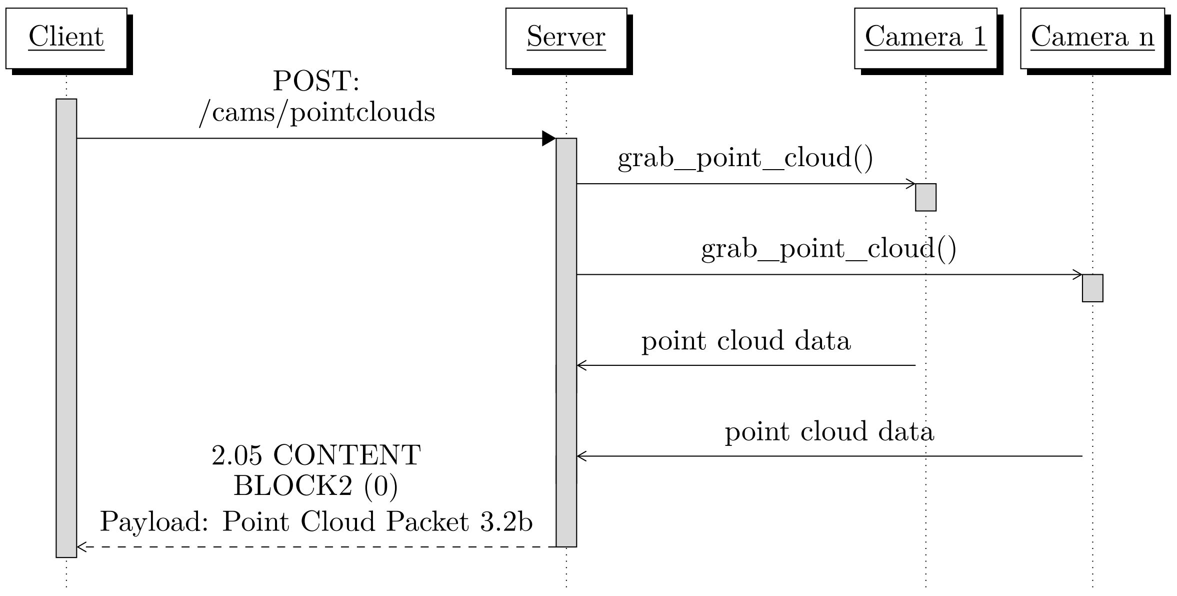

Figure 3.4: CoAP message flow of a successful retrieval of all point clouds from all cameras connected to a single endpoint

to initiate the transmission of a color image.

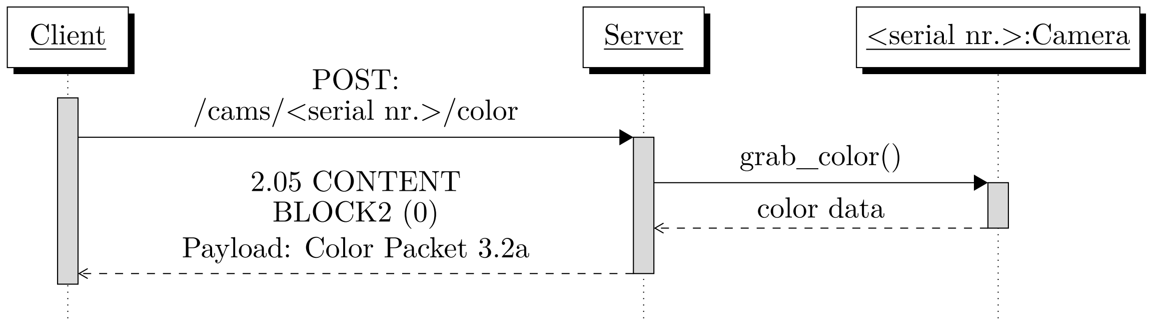

Figure 3.5: CoAP message flow of a successfully initiated transmission of a color image

Resource: /cams/<serial nr.>/depth

This resource is used to retrieve a new depth frame from the camera with the serial number <serial nr.>. Only the `POST` method can be applied to this resource. Upon success CoAP block-wise transfer with the `BLOCK2` option is involved. Figure 3.5 shows the message flow to initiate the transmission of a depth image.

Resource: /cams/<serial nr.>/pointcloud

This resource is used to retrieve a new point cloud from the camera with the serial number <serial nr.>. Only the `POST` method can be applied to this resource. Upon success CoAP

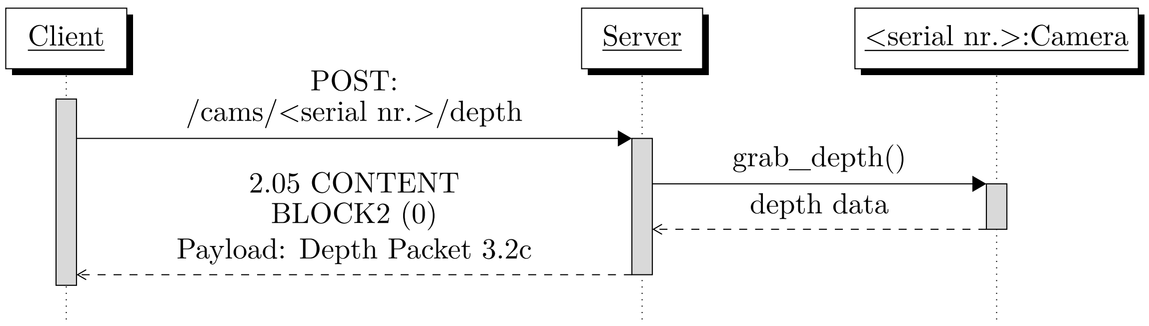

Figure 3.6: CoAP message flow of a successfully initiated transmission of a depth image

block-wise transfer with the `BLOCK2` option is involved. Figure 3.7 shows the message flow to initiate the transmission of a point cloud.

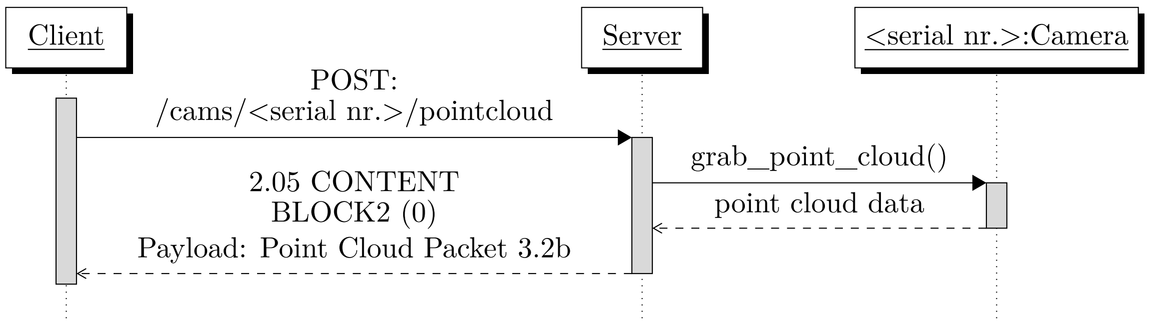

Figure 3.7: CoAP message flow of a successfully initiated transmission of a point cloud

Resource: /cams/<serial nr.>/color-settings

This resource is used to configure the color sensor of the RealSense camera with the serial number <serial nr.>. The `PUT` method is used to update the color sensor configuration and `GET` is used to retrieve the current color sensor configuration. Payload is encoded in JSON, as shown in Listing A.2. The sequence diagram in Figure 3.8 depicts the message flow of a successful query of the current color sensor configuration of a certain camera. The sequence diagram in Figure 3.9 shows the message flow of a successfully performed update of the color sensor settings resource. The message flow is similar for all other configuration resource, with respect to the URI. Supported formats are RGB8, BGR8, RGBA8 and BGRA8. FPS can be 6, 15, 30 or 60. The resolution can be up to 1920x1080 pixels but only up to 30 FPS. In case the demanded configuration cannot be applied a `4.00 BAD REQUEST` response is returned.

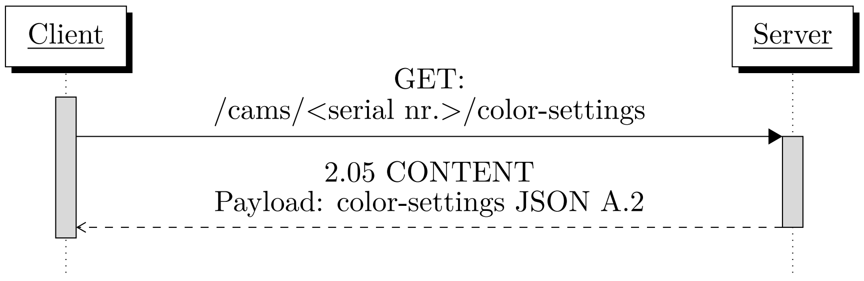
Client
Server
GET:
/cams/<serial nr.>/color-settings
2.05 CONTENT
Payload: color-settings JSON A.2

Figure 3.8: CoAP message flow of a successful retrieval of the color-settings resource of a certain camera

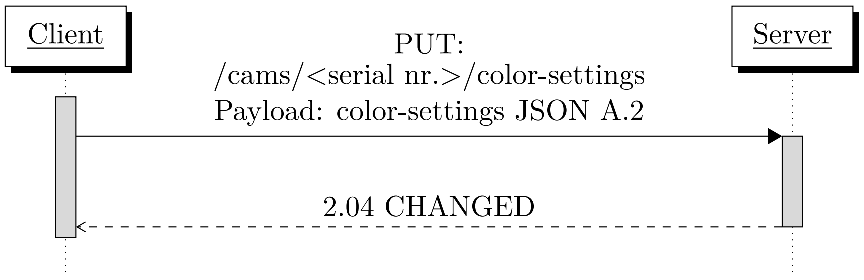
Client
Server
PUT:
/cams/<serial nr.>/color-settings
Payload: color-settings JSON A.2
2.04 CHANGED

Figure 3.9: CoAP message flow of a successful update of the color-settings resource of a certain camera

Resource: /cams/<serial nr.>/depth-settings

This resource is used to configure the depth sensor of the RealSense camera with the serial number <serial nr.>. The `PUT` method is used to update the depth sensor configuration and `GET` is used to retrieve the current depth sensor configuration. Payload is encoded in JSON, as shown in Listing A.1. The only supported format is actually 16 bit unsigned integer depth encoding, Z16, but further formats could be possible in the future. FPS can be 6, 15, 25, 30, 60 or 90. The resolution can be up to 1280x720 pixels but only up to 30 FPS. In case the demanded configuration cannot be applied a `4.00 BAD REQUEST` response is returned. The z-coordinate in meters of a point is computed by $z = depth\_scale * depth\_value$ [47]. Lowering the camera's depth scale means to increase depth accuracy, while the domain of perceptible depth becomes smaller. For example, let the depth scale be the default value 0.001. The maximum depth value is 65 535. So the theoretically maximum z-coordinate would be $0.001 * 65535 = 65.535$ which corresponds to approximately 65 m. However, millimeter accuracy should fit just fine for most applications.

Resource: /cams/<serial nr.>/application-config

The application-config resource should be used to set a 3D region of interest to filter point outliers and a 2D region of interest for images. It can be used to set grab timeout limits in milliseconds, to enable a point cloud registration via an ICP algorithm and to enable some *librealsense* post processing blocks [34]. Those post processing modules are a decimation filter, a spatial filter and a hole filling filter. The decimation filter performs some subsampling according to neighboring pixels and reduces the x and y resolution resulting in less points.

The spatial filter is used to reduce depth noise while it computes the exponential moving average of depth values in x and y dimensions. A point is not smoothed if the difference between it's depth and the current moving average value exceeds a certain threshold. Then the current point's depth becomes the new moving average. This prevents object edges from being smoothed. Lastly, a hole filling filter can be enabled. That is used to interpolate missing depth values by neighboring pixels. There is a temporal filter provided by the RealSense library to interpolate missing depth values from past frames. Since streaming is not done in this application, past frames are not saved and no temporal filtering can be done. Currently filtering is only done with default parameters [47] for each processing block. As suggested by the RealSense post processing paper [34], the applications performs post processing in the order shown in Figure 3.10. The resource is encoded in JSON, as shown in Listing A.3.

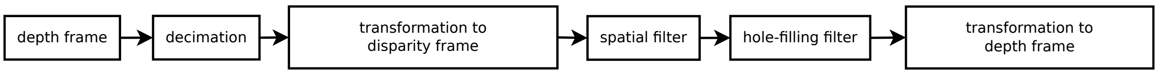
depth frame
decimation
transformation to disparity frame
spatial filter
hole-filling filter
transformation to depth frame

Figure 3.10: Recommended post processing order of a depth frame from a RealSense D400 camera

Resource: /cams/<serial nr.>/3d-transformation

This resource holds the camera specific transformation parameters, which can be set with `PUT` and queried with `GET`. They consist of a rotation matrix, a translation vector, a post rotation vector (roll, pitch, yaw) and a post translation vector, all encoded in JSON. These parameters transform the point cloud obtained from the related camera into a new coordinate system. This transformation is mandatory for proper measurements because measuring results highly depend on the accuracy of rotation matrix and translation vector. Section 3.3.4 explains how these parameters can be obtained. Although, CoAP block-wise transfer is not necessary here, it can be used with the `BLOCK1` and `BLOCK2` option because the JSON file is about 400 B large. An example payload is shown in Listing A.4.

Resource: /cams/<serial nr.>/advanced-config

This resource can be used with `PUT` and `GET` to update and query various camera parameters. The RealSense library provides a convenient way to fine tune their D400 cameras with a JSON file that can be generated with a library provided program, called *realsense-viewer*. In the *realsense-viewer* application one can adjust every camera parameter until they fit the application purpose and export them in a JSON file. There also exist camera presets [47], which are a set of parameters that have proven to deliver best results for specific application. For example the preset “High Accuracy” is best suited for applications where it is better to have no depth value than to have a low confidential depth value, which could be the case in some robotics applications. The JSON file can be applied with the `rs2_load_json()` function. If it fails to apply the JSON parameters, a `4.00 BAD REQUEST` is returned in a response. The JSON file is about 3.5 kB large, hence CoAP block-wise transfer is required.

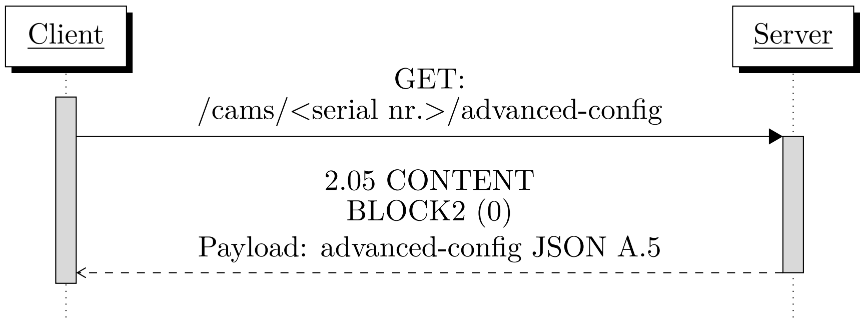
Client
Server
GET:
/cams/<serial nr.>/advanced-config
2.05 CONTENT
BLOCK2 (0)
Payload: advanced-config JSON A.5

Figure 3.11: CoAP message flow of a successful retrieval of the advanced-config resource of a certain camera

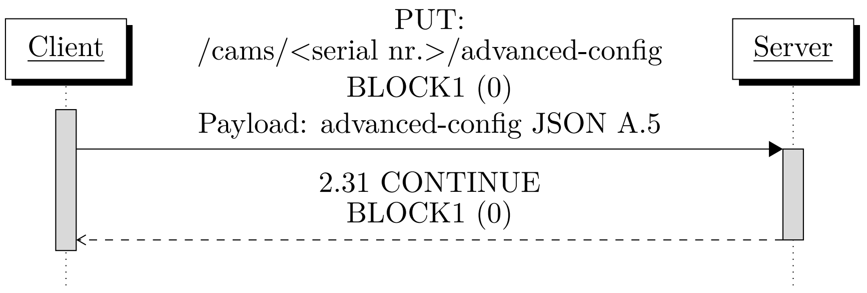
Client
Server
PUT:
/cams/<serial nr.>/advanced-config
BLOCK1 (0)
Payload: advanced-config JSON A.5
2.31 CONTINUE
BLOCK1 (0)

Figure 3.12: CoAP message flow of a successful update of the advanced-config resource of a certain camera

A successful retrieval of this resource is shown in Figure 3.11 and a successful resource update is shown in Figure 3.12. An example payload is shown in Listing A.5.

3.3.4 3D-Transformation

To have each point from all cameras defined relatively to a common origin it is necessary to perform a 3D-Transformation [38]. For each point x, the transformed point x' is computed with

$$x' = R * x + t \tag{3.1}$$

, where $x, x', t \in \mathbb{R}^3$, $R \in \mathbb{R}^{3\times3}$. A separate program in C++ has been written to compute *rotation matrix R* and *translation vector t*. The C++ library *ArUco* can be used to estimate the camera pose relative to an *ArUco* marker that is detected in a color image. Using a single marker to estimate the camera's pose can be error prone [48]. Thus the *ArUco* library provides a tool to create a marker map, `aruco_create_markermap`. A marker has an ID, a center and four corners in pixel coordinates. There are different kinds of markers which are grouped in dictionaries. For this application the `ARUCO_MIP_36h12` dictionary has been used. The camera pose relative to the marker is described as a translation vector t_{MC} and a rotation vector $rvec_{MC}$ which are the results of `solvePnP()` from *OpenCV* [49]. The rotation vector $rvec_{MC}$ can be converted to a rotation matrix R_{MC} with the `Rodrigues()` function from *OpenCV* as well. Let x_M be a point in the marker coordinate system. The point x_M can be transformed to the camera coordinate system with Equation 3.2.

$$x_C = R_{MC} \times x_M + t_{MC} \tag{3.2}$$

To get the opposite direction from the camera coordinate system to the marker coordinate system, Equation 3.2 must be converted to Equation 3.6.

$$
\begin{aligned}
x_C &= R_{MC} \times x_M + t_{MC} && (3.3) \\
x_C - t_{MC} &= R_{MC} \times x_M && (3.4) \\
R_{MC}^{-1} \times (x_C - t_{MC}) &= x_M && (3.5) \\
x_M &= R_{MC}^{-1} \times x_C - R_{MC}^{-1} * t_{MC} && (3.6)
\end{aligned}
$$

The resulting rotation matrix R_{CM} to transform a point from the camera coordinate system to the marker coordinate system is R_{MC}^{-1} and the resulting translation vector t_{CM} to transform a point from the camera coordinate system to the marker coordinate system is $-R_{MC}^{-1} * t_{MC}$. Before $rvec_{MC}$ and $tvec_{MC}$ can be computed *ArUco* must be provided with the camera Intrinsic Parameters of the color sensor. That are a camera matrix C 3.3.4 and a tupel d of five distortion values. Both can be obtained from a camera calibration.

$$
C = \begin{pmatrix} f_x & 0 & c_x \\ 0 & f_y & c_y \\ 0 & 0 & 1 \end{pmatrix}
$$

The parameter f_x is the Focal Length in multiples of pixel x-length, f_y is the Focal Length in multiples of pixel y-length, c_x is the x pixel coordinate of the Principal Point and c_y is the y pixel coordinate of the Principal Point. Intrinsic Parameters are stored on the camera and have been estimated when the camera has been factory calibrated [36]. They are not the same for the same camera model, thus each camera needs an individual calibration. The quality of the calibration parameters varies from camera to camera. While the camera with serial number 809512060141 does not have very accurate parameters, the points from the camera with serial number 840412060746 transform very well with factory determined parameters. A recalibration of a camera is possible but not as accurate as can be done with professional equipment. Even though Intel provides a paper and a calibration framework [36], self-determined parameters from 100 images resulted in worse results. The RealSense library provides an interface to query the intrinsic camera parameters, `rs2_get_video_stream_intrinsics()`. The distortion coefficients returned by that function are always zero. So it can be assumed that frames automatically become rectified by the library. However, there must be distortion. The real distortion coefficients for the left and right imagers can be queried with an external tool that is mentioned in the camera calibration white paper from Intel. But distortion coefficients for the RGB sensor are not provided by Intel. To read the camera calibration from the device the *CustomRW* tool from Intel can be used with `CustomRW -sn <serial nr.> -r -f <outfile.xml>`.

The transformation tool takes as arguments: the configuration file for the generated marker map, the actual marker size in meters e.g. printed on a sheet of paper, the serial number of the camera, the file that contains the Intrinsic Parameters, width resolution, height resolution, a number of threads that shall be used to transform all points and an output file. The *librealsense pipeline* API is used to start streaming color and depth frames from a RealSense camera and *ArUco* tries to detect the configured marker map in the color image. When the marker map could be detected successfully, transformation parameters R_{CM} and t_{CM} were computed. These parameters hold for the transformation from the color sensor to the marker map center, but each point in a point cloud from a D400 RealSense camera is defined relative to the left imager, so the extrinsic transformation parameters from the left imager to the color sensor must be applied as well. The Extrinsic Parameters from the imagers to the color sensor and vice versa have also been stored on the camera at the time of factory calibration and can be queried with the `rs2_register_extrinsics()` function. Let R_1 be the rotation matrix from the left imager to the color sensor and t_1 the transformation vector from the left imager to the color sensor. Let R_2 be the rotation matrix from the color sensor to the marker map and t_2 the transformation vector from the color sensor to the marker map. A point x in the camera coordinate system is transformed to x' in the marker coordinate system, as shown in Equation 3.8.

$$\begin{aligned} x' &= R_2 \times (R_1 \times x + t_1) + t_2 \qquad (3.7)\\ &= R_2 \times R_1 \times x + R_2 \times t_1 + t_2 \qquad (3.8) \end{aligned}$$

If the tool was compiled with `make WITH_GRAPHICS=1` then the transformed points are visualized with *OpenGL* [50] and *GLEW* [51] and the user will be able to apply manual correction, with respect to rotation, translation and scaling. Manual changes in rotation are stored as roll, pitch and yaw values in degrees, where roll is the rotation around the x-axis, pitch is the rotation around the y-axis and yaw is the rotation around the z-axis, with respect to the object coordinate system. The result should be that the world axis lie in the center of the marker map, with the z-axis perpendicular. Other library dependencies are `GLFW` [52] to create a window and to capture user input and `glm` [53] for matrix computations. For an embedded device the tool should not be compiled with extra graphical support. The tool produces an output file in JSON that lists ``` ``rotation_matrix'' ``` and ``` ``translation_matrix'' ``` as the result of the computed transformation and ``` ``post_rotation_matrix'' ``` (roll, pitch , yaw) and ``` ``post_translation_matrix'' ``` as the result of the manual correction. A ``` ``scale_matrix'' ``` and a ``` ``post_scale_matrix'' ``` are also contained in the file but not needed for the application of this thesis. Figure 3.13 shows the transformation result.

3.3.5 Image Processing

In order to compute object dimensions, some image processing has to be done by the client. The client application depends on *OpenCV* [49] with a version prior to 4.0.0 because since the release of *OpenCV* 4.0.0 the compilation standard has been raised to C++ 11 and the C API has been dropped.

It is assumed that all cameras are facing the ground and have been configured to use a common coordinate system with the z-axis pointing upwards and is oriented perpendicular to the ground. The measuring area should be free of any other object that shall not be measured because only one object can be measured at a time. In advance a minimum z value for all points of interest should have been configured in the application-config resource from Subsection 3.3.3 for all cameras because points that represent the ground should not be transmitted by the server. The only points of interest for the computation are those which form the upper surface of the object within the measuring range. The object's z dimension is computed as the maximum observed z-value from the points that form the upper surface. To compute x and y dimensions only the x and y components of a point are considered. From these 2D points the convex hull is computed with *OpenCV's* `cvConvexHull2()` function. The resulting points are then used as input to *OpenCV's* `cvMinAreaRect2()` function which

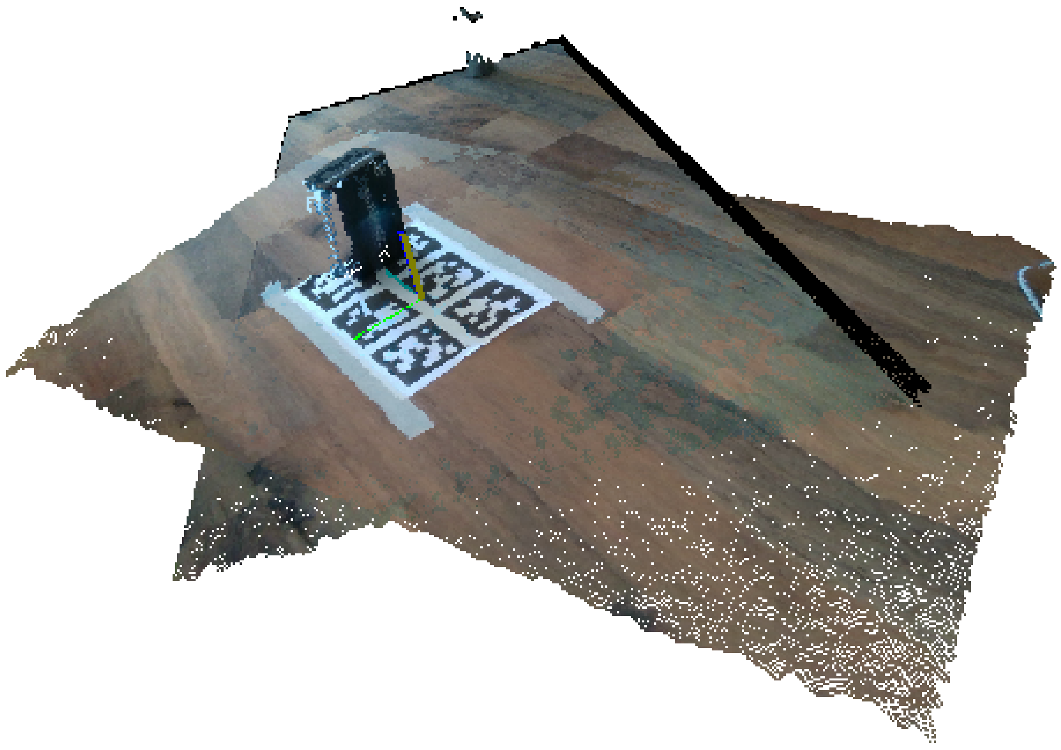

Figure 3.13: Aligned point clouds after 3D transformation

computes the minimum area rectangle that encloses all points. The rectangle's width and height are the x and y dimensions of the object below the sensors.

3.4 Experiments

This section is dedicated to the performance analysis of the presented application that provides color, depth and point cloud data from RealSense D400 cameras as CoAP resources. The experiments only cover the color and point cloud resource of a single camera but not the depth image resource because the depth image is just a prestage of the point cloud. Experimental parameters are hardware, resolution and network overhead. Tests have been executed on a desktop computer and on embedded hardware. Because performance strongly depends on the CoAP library, *libcoap* has been used as a well known library reference. As a test scenario, a client initiates the block-wise transfer of the requested resource 32 times, with the maximum block size of 1024 B [18]. After each transmission of a complete image or point cloud, the client sleeps for one second. For each test case, transmission times and moving average transmission times for each complete resource transmission are measured. The term "transmission time" is defined to be the elapsed time from request transmission to the last successfully received response which completes the transmission of a resource. Hence, "transmission time" includes processing delay which includes the time it takes to grab an image. The average time from 32 grabs of a color image has been measured with ca. 0.1 s, while the average time to grab a depth frame and to calculate the point cloud has been measured with ca. 0.185 s. Server statistics, i.e. user CPU time, system CPU time and maximum resident set size, are obtained with `getrusage()`. Some test cases have been repeated with `valgrind --tool=callgrind --simulate-cache=yes` to capture the number of executed instructions, instruction miss rate, data accesses and data access miss rate. Table 3.2 lists the hardware that has been used. The application has been compiled with `clang -O3`.

Name:	Desktop	Lenovo-Yoga L390	Odroid-Xu4
OS:	Ubuntu 18.04	Arch Linux	Ubuntu 18.04
Kernel:	4.15.0-48-generic	5.0.3-arch1-1-ARCH	4.14.111-158
CPU:	i5-4460 - 3.20GHz	i5-8265U - 1.6GHz	SAMSUNG Exynos 5422
Cores:	4	8	8
RAM:	8GB DDR3	8GB DDR3	2GB LPDDR3
Network:	802.11n - 2.4GHz	802.11n - 2.4GHz	Ethernet

Table 3.2: Hardware that has been used in all test cases

3.4.1 Test Case 1: (Color, 640x480, local)

In the first test case the camera has been configured to produce color frames at a resolution of 640x480 pixels in BGR8 format. Server and client application both have been running on the same desktop computer from Table 3.2. $640 \times 480 \times 3\,\mathrm{B} + 10\,\mathrm{B}$ header result in

921 610 B of CoAP response payload to be transferred 32 times. This test case has also been repeated with Callgrind.

3.4.2 Test Case 2: (Color, 1280x720, local)

The second test case shows how the color image resolution affects the measured parameters. The camera has been configured to produce color frames at a resolution of 1280x720 pixels in BGR8 format. Server and client application both have been running on the same desktop computer from Table 3.2. $1280 \times 720 \times 3\,\mathrm{B} + 10\,\mathrm{B}$ header result in 2 764 810 B of CoAP response payload to be transferred 32 times. Because the resolution in test case 2 is 2 times higher than in test case 1, the average response time is expected to be thrice as much as in test case 1. This test case has also been repeated with Callgrind.

Hypothesis 1 (H1): *The average transmission time in test case 2 will be at most thrice as much as in test case 1.*

Hypothesis 2 (H2): *The number of instructions in test case 2 will be at most thrice as high as in test case 1.*

Hypothesis 3 (H3): *The maximum resident set size in test case 2 will be at most thrice as much as in test case 1.*

3.4.3 Test Case 3: (libcoap, 2764810 Byte, local)

The same amount of data as in test case 2 has been transferred in this test case but *libcoap* has been used as a CoAP library reference to illuminate the influence of the CoAP library and the CoAP block-wise transfer implementation. To make test case 3 comparable with test case 2, server and client both have been running locally on the same machine as in test case 2. For hypothesis, see test case 8 in Subsection 3.4.8.

3.4.4 Test Case 4: (Color, 1280x720, 1-Hop)

Test case 4 is a repetition of test case 2 but this time in a wireless network scenario. The server has been running on the desktop computer and the client has been running on the Lenovo Yoga L390, both listed in Table 3.2.

Hypothesis 4 (H4): *The average transmission time in test case 4 will be higher than the average transmission time in test case 2 and transmission times will have a greater variance.*

Hypothesis 5 (H5): *The maximum resident set size in test case 4 will be approximately as large as the maximum resident set size in test case 2.*

3.4.5 Test Case 5: (Embedded, Color, 1280x720, 1-Hop)

Test case 5 is a repetition of test case 4, where the server has been running on an Odroid-Xu4 and the client has been running on the desktop computer. Test case 5 is not fully comparable to test case 4 because the Odroid does not have a WiFi interface.

Hypothesis 6 (H6): *The average transmission time in test case 5 will be higher than the average transmission time in test case 4.*

Hypothesis 7 (H7): *The maximum resident set size in test case 5 will be approximately as large as the maximum resident set size in test case 4.*

3.4.6 Test Case 6: (Point Cloud, 640x480, local)

In the 6th test case the camera has been configured to produce point clouds from depth images at a resolution of 640x480 pixels in Z16 format. Server and client application both have been running at the same desktop computer from Table 3.2. The observed number of valid points has been approximately 286 000. 286 000 points × 12 B per point + 12 B header result in 3 432 012 B of response CoAP payload to be transferred 32 times. This test case has also been repeated with Callgrind.

Hypothesis 8 (H8): *The average transmission time in test case 6 will be greater than the average transmission time in test case 1.*

Hypothesis 9 (H9): *The maximum resident set size in test case 6 will be greater than the maximum resident set size in test case 1.*

Hypothesis 10 (H10): *The number of instructions in test case 6 will be higher than the number of instructions in test case 1.*

3.4.7 Test Case 7: (Point Cloud, 1280x720, local)

Test case 7 shows how the depth image resolution affects the measured parameters. The camera has been configured to produce point clouds from depth frames at a resolution of 1280x720 pixels in Z16 format. Server and client application both have been running on the same desktop computer from Table 3.2. The observed number of valid points has been approximately 836 000. 836 000 points × 12 B per point + 12 B header result in 10 032 012 B of CoAP response payload to be transferred 32 times. This test case has also been repeated with Callgrind.

Hypothesis 11 (H11): *The average transmission time in test case 7 will be at most thrice as much as in test case 6.*

Hypothesis 12 (H12): *The number of instructions in test case 7 will be at most thrice as high as in test case 6.*

Hypothesis 13 (H13): *The maximum resident set size in test case 7 will be at most thrice as much as in test case 6.*

3.4.8 Test Case 8: (libcoap, 10032012 Byte, local)

In test case 8 *libcoap* has again been used to serve as a CoAP library reference implementation to transfer 10 032 012 B via block-wise transfer.

Hypothesis 14 (H14): *libcoap will have similar transmission times to the custom CoAP library.*

Hypothesis 15 (H15): *libcoap will need less memory than the custom CoAP library.*

3.4.9 Test Case 9: (Point Cloud, 1280x720, 1-Hop)

In test case 9 a point cloud from a depth frame at a resolution of 1280x720 pixels in Z16 format has been transmitted over 1 hop in a wireless network, 32 times. The server has been the desktop PC and the client has been the Lenovo laptop from Table 3.2.

Hypothesis 16 (H16): *The average transmission time in test case 9 will be higher than the average transmission time in test case 7 and transmission times will have a greater variance.*

Hypothesis 17 (H17): *The maximum resident set size in test case 9 will be approximately as large as the maximum resident set size in test case 7.*

3.4.10 Test Case 10: (Point Cloud, Decimation, 1280x720, 1-Hop)

The RealSense library provides a decimation filter to reduce the number of points in a point cloud. This test has been accomplished to show the influence of post processing with respect to the measured parameters.

Hypothesis 18 (H18): *The average transmission time in test case 10 will be lower than the average transmission time in test case 9.*

Hypothesis 19 (H19): *The maximum resident set size in test case 10 will be approximately the same as in test case 9.*

3.4.11 Test Case 11: (Embedded, Point Cloud, Decimation, 1280x720, 1-Hop)

To complete all test cases, the 11th test case repeats test case 10 with the Odroid-Xu4 as a CoAP server and the desktop computer as a CoAP client.

Hypothesis 20 (H20): *The average transmission time in test case 11 will be higher than the average transmission time in test case 10.*

Hypothesis 21 (H21): *The maximum resident set size in test case 11 will be approximately the same as in test case 10.*

CHAPTER 4

Thesis Outcome

In this chapter, the test cases from the previous chapter are evaluated. At the end of Section 4.1 there are evaluation charts in Subsection 4.1.12 that show each test case, compared to each other, with respect to one measured parameter.

4.1 Evaluation

This section evaluates the described test cases from the previous section. There is a short table that summarizes rounded values of the minimum, maximum and average transmission time, standard deviation and the coefficient of variance for each test case. The transmission times mark an upper bound because as described in Subsection 3.3.5, only the upper surface is needed to compute the object dimensions. It is up to the user to configure a 3D measuring rage with the resource shown in Subsection 3.3.3 to limit the number of points that actually need to be transmitted. Measurements of the time spent in user space and kernel space are inaccurate. Instead, Callgrind is a better measure of program complexity.

4.1.1 Evaluation Test Case 1: (Color, 640x480, local)

Except for the first transmission which almost took 0.6 s, all local transmissions of a 640x480 color image have been completed within 0.11 s and 0.14 s. The transmission times are expectedly small and there is almost no variance. The rolling average transmission time tends to decrease. For the last transmission the average was about 0.138 s. The maximum resident set size after all transmissions was 138 624 kB. When the test has been repeated with Callgrind, 10 484 381 115 instruction- and 2 619 011 862 data references have been measured, where the I1 miss rate was 0.06%, D1 miss rate was 0.2% and LLD miss rate was 0.01%. The program has almost spent twice as much time in system space than in user space.

Min. [ns]	Max. [ns]	Avg. [ns]	SD. [ns]	Coefficient Of Variance
114 601 127	597 480 766	137 930 475	82 792 576	0.60

Table 4.1: Statistic of transmission times for test case 1: (Color, 640x480, local)

4.1.2 Evaluation Test Case 2: (Color, 1280x720, local)

Like in test case 1, with more than 0.6 s the first transmission took longer than all others, which lie in an interval between 0.16 s and 0.21 s. After the last transmission, the average transmission time was about 0.2 s. It can be concluded that scaling the image resolution does not significantly increase the local transmission time. The maximum resident set size was 386 908 kB, which is roughly 2.8 times the maximum resident set size of test case 1. Callgrind reported 16 701 246 075 instruction- and 4 008 742 996 data references. The I1 miss rate was 0.1%, D1 miss rate was 0.4% and LLD miss rate was 0.3%. Thus references and miss rates have increased. The program has spent more time in system space than in user space but less than twice as much.

Min. [ns]	Max. [ns]	Avg. [ns]	SD. [ns]	Coefficient Of Variance
165 467 471	643 246 091	201 034 821	79 797 913	0.4

Table 4.2: Statistic of transmission times for test case 2: (Color, 1280x720, local)

Hypothesis **H1**, **H2** and **H3** are true.

4.1.3 Evaluation Test Case 3: (libcoap, 2764810 Byte, local)

Transmitting the same amount of data with *libcoap* shows a significant increase of transmission time. A single transmission of about 2.8 MB consistently takes 24.8 s up to 26.3 s. In contrast *libcoap* consumes very little memory. The maximum resident set size has been measured with 12 484 kB. The long latency may result from the complexity of *libcoap* and developers might focus more on memory minimization than on latency. The library has also spent roughly 240 times longer in user space than in system space.

Min. [ns]	Max. [ns]	Avg. [ns]	SD. [ns]	Coefficient Of Variance
24 817 575 651	26 308 355 473	25 479 611 952	434 925 136	0.02

Table 4.3: Statistic of transmission times for test case 3: (libcoap, 2764810 Byte, local)

4.1.4 Evaluation Test Case 4: (Color, 1280x720, 1-Hop)

Transmission time was measured within an interval of 10 s and 65 s with a median of 14.7 s. The average transmission time decreased to 17 s. Thus, test case 4 shows higher transmission times and a higher variance because this test introduces a wireless network. The maximum resident set size was, compared to test case 2, surprisingly small with 69 000 kB, which is still very large compared to *libcoap*. The server application has spent more than twice as much time in system than in user space.

Min. [ns]	Max. [ns]	Avg. [ns]	SD. [ns]	Coefficient Of Variance
10 470 965 550	64 788 622 316	16 921 158 259	9 460 257 807	0.56

Table 4.4: Statistic of transmission times for test case 4: (Color, 1280x720, 1-Hop)

Hypothesis **H4** is true but **H5** is false.

4.1.5 Evaluation Test Case 5: (Embedded, Color, 1280x720, 1-Hop)

When the server was running on the Odroid-Xu4, transmission times have been captured within 8.7 s and 17.6 s. On average a transmission of a color frame took 10.8 s. The median was 10.5 s. The smaller latency results from the Ethernet connection. The maximum resident set size was 77 724 kB which is close to that of test case 4. The time spent in system space was about 30% higher than the time spent in user space.

Min. [ns]	Max. [ns]	Avg. [ns]	SD. [ns]	Coefficient Of Variance
8 779 341 489	17 562 543 770	10 845 170 654	1 893 791 200	0.17

Table 4.5: Statistic of transmission times for test case 5: (Embedded, Color, 1280x720, 1-Hop)

Hypothesis **H6** is false and **H7** is true.

4.1.6 Evaluation Test Case 6: (Point Cloud, 640x480, local)

As can be observed from test case 6 the transmission of a point cloud does take longer than a color frame in test case 1. That follows from more computational overhead to produce a point cloud from a depth image and a larger amount of transmission data. Transmission latency has been observed within an interval of 0.26 s and 0.34 s where the median was about 0.27 s. The average latency after all 32 transmissions was 0.276 s. The maximum resident set size increased up to 470 000 kB. While the test was running, the program spent more than 30% longer in system space than in user space. A repetition of this test case with Callgrind showed 9 799 934 889 instruction references, where I1 miss rate was 0.21%.

There have been measured 2 208 025 980 data references, where the D1 miss rate was 0.9% and the LLD miss rate was 0.6%.

Min. [ns]	Max. [ns]	Avg. [ns]	SD. [ns]	Coefficient Of Variance
264 153 682	332 764 469	276 228 236	15 023 430	0.05

Table 4.6: Statistic of transmission times for test case 6: (Point Cloud, 640x480, local)

Hypothesis **H8** and **H9** are true and **H10** is false.

4.1.7 Evaluation Test Case 7: (Point Cloud, 1280x720, local)

Test case 7 shows that the increase of depth image resolution has a higher impact on transmission time than it has for color images. Transmission times are within 0.42 s and 0.62 s. The median was 0.44 s and the average transmission time was 0.45 s. The maximum resident set size grew up to 1.398 GB. The server has spent 12% more in system space than in user space. Callgrind reported 20 266 928 023 instruction references and 4 259 744 475 data references. The I1 miss rate was 0.34%, D1 miss rate was 1.2% and LLD miss rate was 0.8%.

Min. [ns]	Max. [ns]	Avg. [ns]	SD. [ns]	Coefficient Of Variance
420 111 008	620 464 002	451 855 799	42 100 481	0.09

Table 4.7: Statistic of transmission times for test case 7: (Point Cloud, 1280x720, local)

Hypothesis **H11**, **H12** and **H13** are true.

4.1.8 Evaluation Test Case 8: (libcoap, 10032012 Byte, local)

On the transmission of approximately the same amount of data as in test case 7 , 10 MB, with *libcoap*, it could be observed that the transmission time lied within an interval of 323 s and 330 s. The median was 323.9 s and the average was 324.1 s. As in test case 3, *libcoap* showed very little memory consumption with a maximum resident set size of 33 820 kB. The server of *libcoap* spent ca. 452 times longer in user space than in system space.

Min. [ns]	Max. [ns]	Avg. [ns]	SD. [ns]	Coefficient Of Variance
323 467 464 410	329 172 966 314	324 110 784 250	1 019 277 940	0.00

Table 4.8: Statistic of transmission times for test case 8: (libcoap, 10032012 Byte, local)

As can be concluded from test case 3 and test case 8, hypothesis **H14** is false and **H15** is true.

4.1.9 Evaluation Test Case 9: (Point Cloud, 1280x720, 1-Hop)

Over 1 hop in a wireless network, transmission times became 150 times higher than in test case 7. The transmission times could be measured within an interval of 39.4 s and 72.7 s. The median was 51 s and the average was 52.4 s. The time spent in system space was more than twice as mus as the time spent in user space. Similar to test case 4, the maximum resident set size became smaller when data was transmitted over WiFi. The maximum resident set size was 108 888 kB.

Min. [ns]	Max. [ns]	Avg. [ns]	SD. [ns]	Coefficient Of Variance
39 429 807 187	72 669 279 561	52 370 609 994	8 603 131 783	0.16

Table 4.9: Statistic of transmission times for test case 9: (Point Cloud, 1280x720, 1-Hop)

Hypothesis **H16** is true and **H17** is false.

4.1.10 Evaluation Test Case 10: (Point Cloud, Decimation, 1280x720, 1-Hop)

For a real industrial use case, the observed transmission times in test case 9 are way to high but the number of points can be reduced with a decimation filter to decrease the amount of transmission data. With the decimation post processing block from *librealsense*, the transmission times could be limited within an interval of 10.5 s and 29.3 s. The median was 16 s and the average transmission time was 16.9 s. Compared to test case 9, the transmission time could be reduced by ca. 68%. The server almost spent twice as long in system space than in user space. The maximum resident set size was 69 208 kB. Hence, resident set size has decreased, compared to test case 9.

Min. [ns]	Max. [ns]	Avg. [ns]	SD. [ns]	Coefficient Of Variance
10 506 655 071	29 272 974 642	16 928 715 709	5 162 878 980	0.30

Table 4.10: Statistic of transmission times for test case 10: (Point Cloud, Decimation, 1280x720, 1-Hop)

Hypothesis **H18** is true and **H19** is false.

4.1.11 Evaluation Test Case 11: (Embedded, Point Cloud, Decimation, 1280x720, 1-Hop)

Test case 11 repeats test case 10 with the server running on an Odroid-Xu4. It could be observed that the transmission times lied within an interval of 9.9 s and 14.9 s, due to the use of Ethernet. The median was 10.9 s and the average was 11.1 s. The maximum resident set size was 74 476 kB. The server has spent approximately 34% longer in system space than in user space.

Min. [ns]	Max. [ns]	Avg. [ns]	SD. [ns]	Coefficient Of Variance
9 928 847 321	14 848 909 781	11 070 906 767	946 185 343	0.09

Table 4.11: Statistic of transmission times for test case 11: (Embedded, Point Cloud, Decimation, 1280x720, 1-Hop)

Hypothesis **H20** is false and **H21** is true.

4.1.12 Evaluation Charts

This subsection shows the results of the experiments in several charts. Each chart compares a subset of all test cases with regards to a single parameter.

Chart: Transmission Times

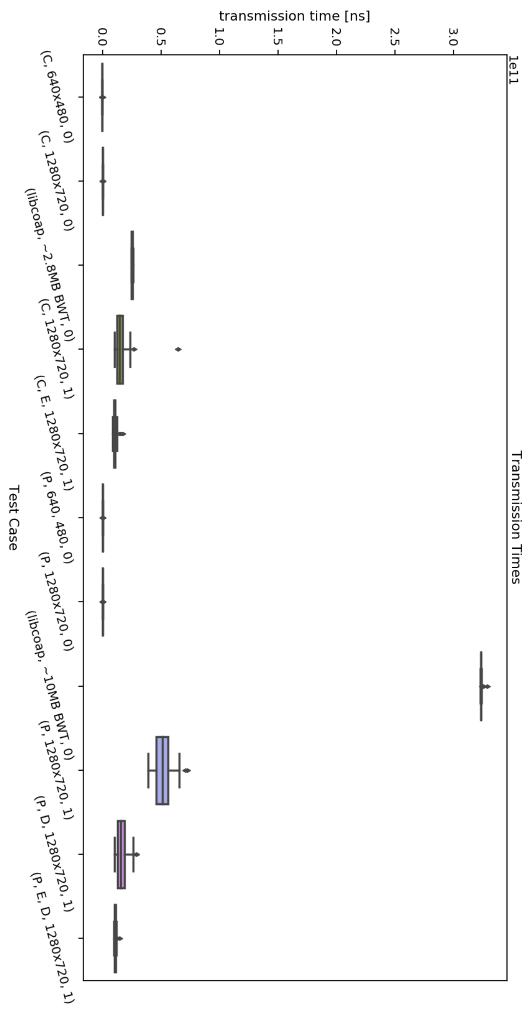

Figure 4.1: Box plot of all transmission times for all test cases

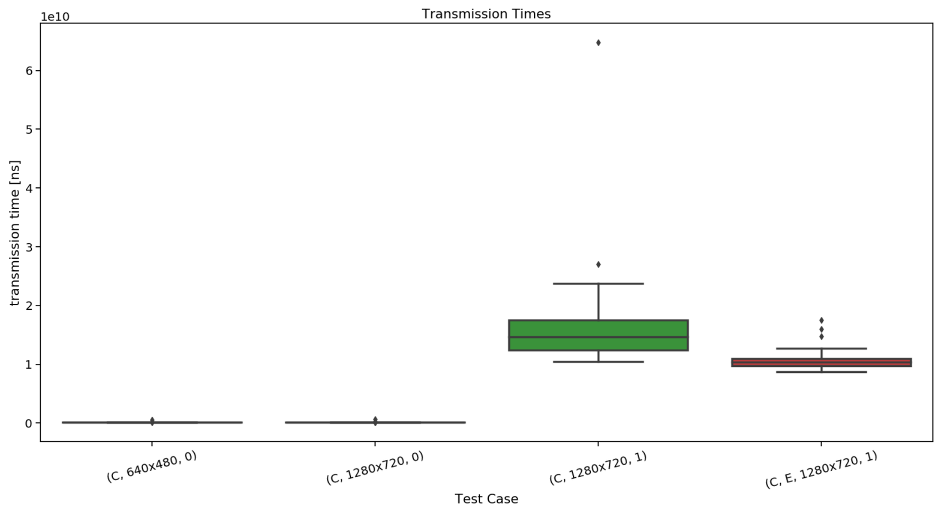

Figure 4.2: Box plot of all transmission times for all color related test cases

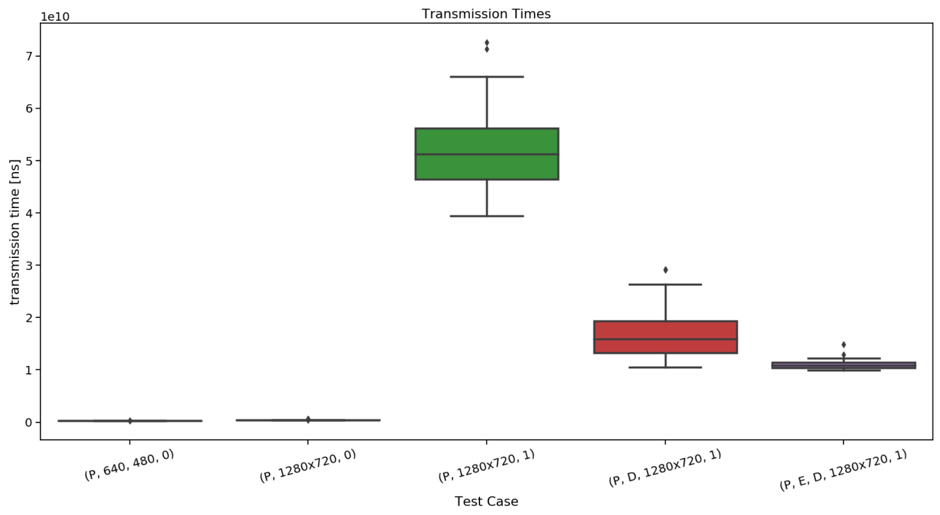

Figure 4.3: Box plot of all transmission times for all point cloud related test cases

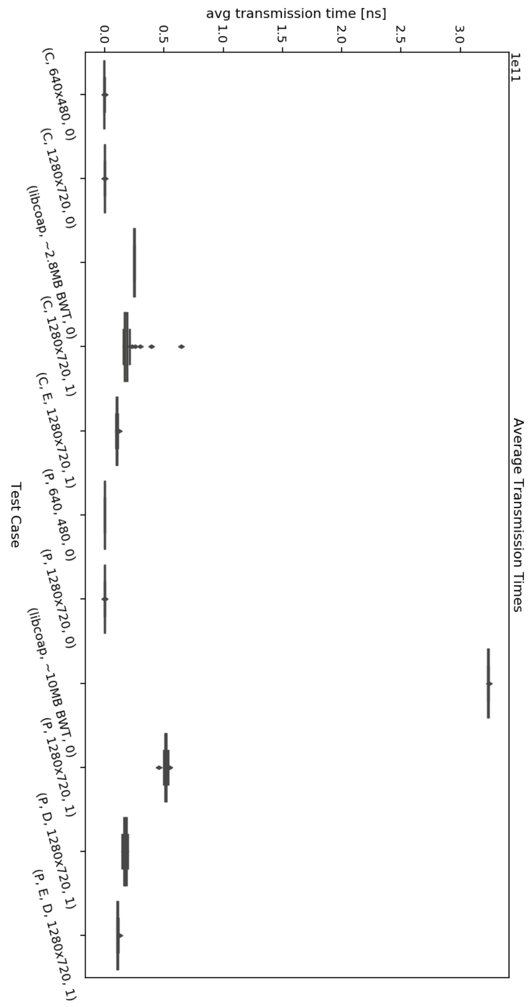

Figure 4.4: Box plot of moving average transmission times for all test cases

Theses box plots show that the transmission times are more heavily affected by the network condition, rather than resolution or hardware. Transmission times are generally higher for point clouds than they are for color images. On a local machine transmission times are very low. For a network, post processing, region filtering and maybe a lower resolution are recommended.

Chart: Maximum Resident Set Size

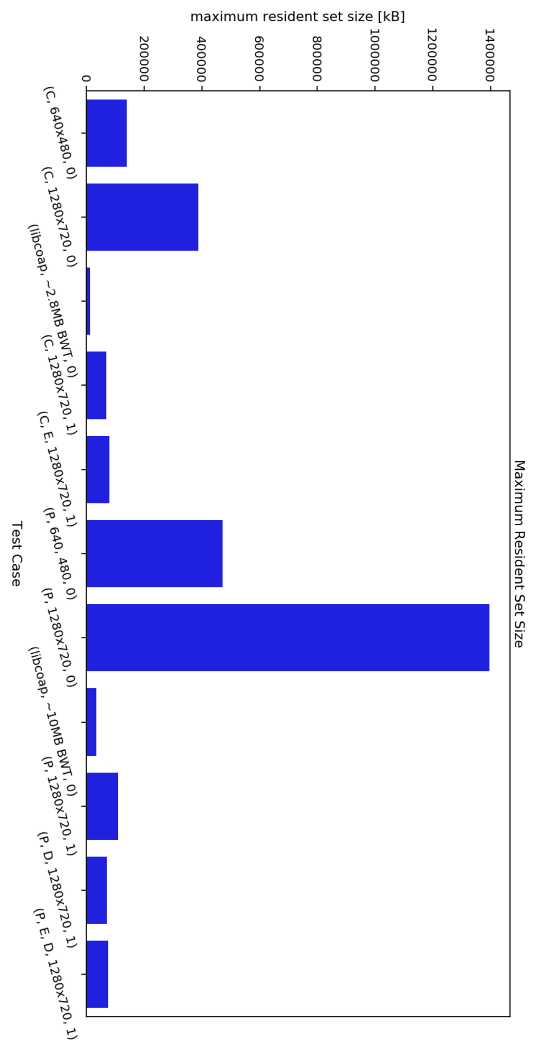

Figure 4.5: Bar chart of maximum resident set size for all test cases

The maximum resident set size was really high, when server and client were running on the same machine. In a network scenario, it became smaller.

Chart: Instruction References

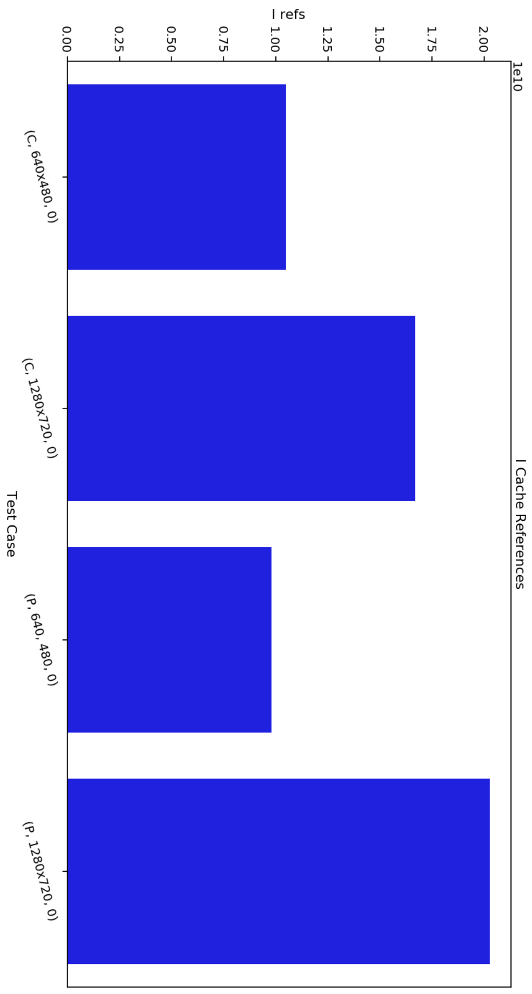

Figure 4.6: Bar chart of instruction references

The number of instructions scales with the resolution but the kind of resource, whether color image or point cloud, does not make much of a difference.

Chart: I1 Cache Miss Rates

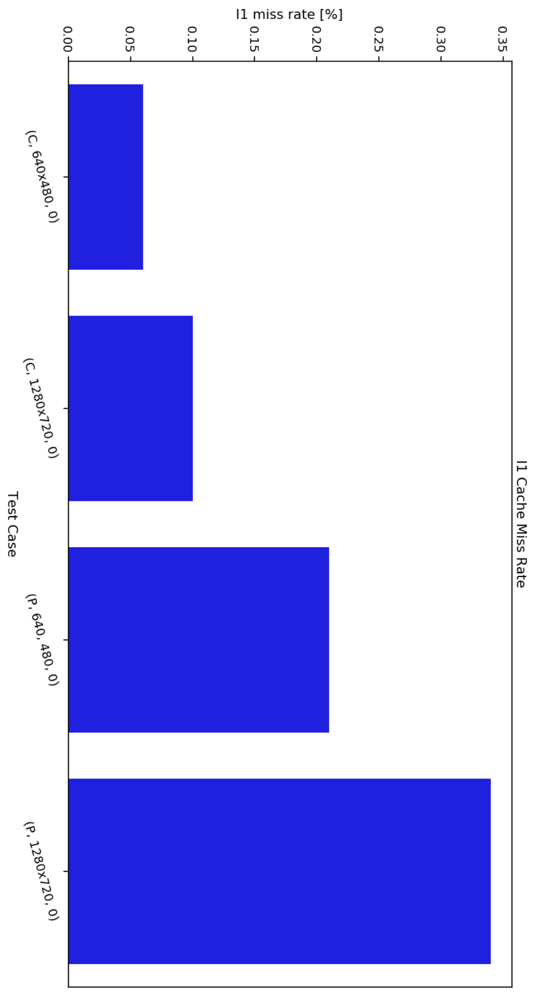

Figure 4.7: Bar chart of I1 miss rate

The instruction cache miss rates are very low as they are always below 1%. The last level instruction cache miss rate has always been zero, so a chart of them has been omitted. The miss rate scales with the resolution and the kind of resource.

Chart: Data References

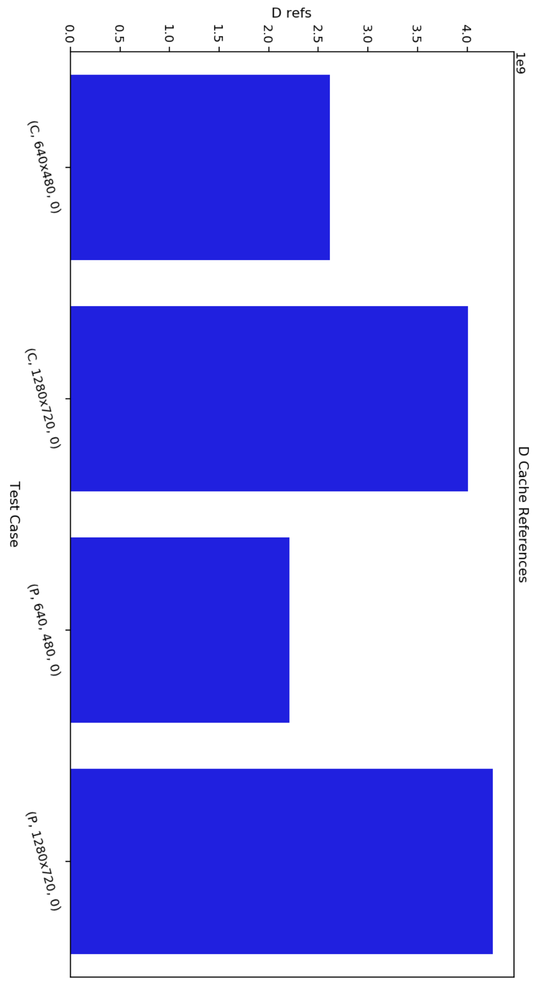

Figure 4.8: Bar chart of data references

As well as the instruction references, the number of data references is most affected by the image resolution.

Chart: D1 Cache Miss Rates

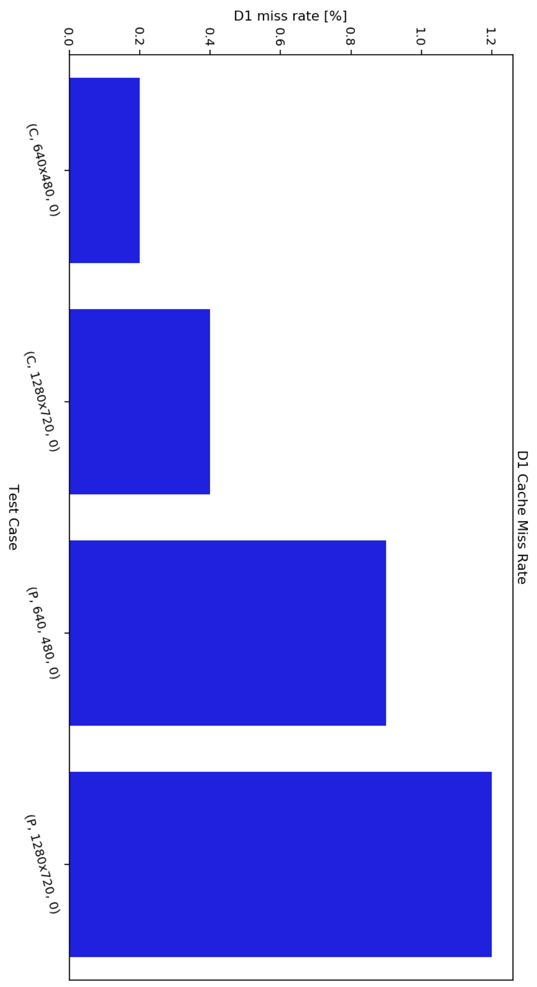

Figure 4.9: Bar chart of D1 miss rate

The D1 cache miss rates are a little higher than the instruction cache miss rates but still acceptable low. They scale with resolution and resource kind.

Chart: LLd Cache Miss Rates

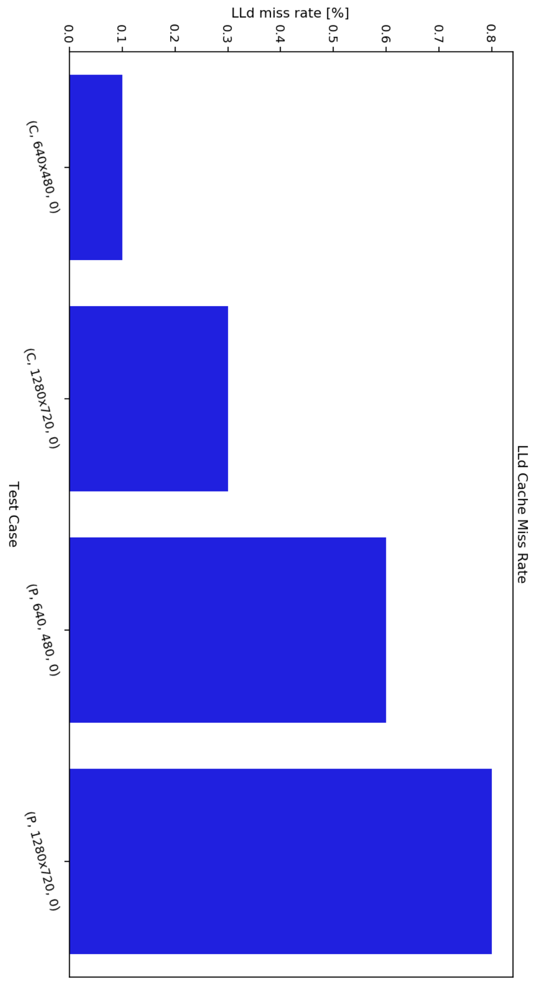

Figure 4.10: Bar chart of LLd miss rate

The last level data cache references are low as well and scale with image resolution and resource kind.

CHAPTER 5

Conclusion

This chapter summarizes the advantages and disadvantages of using CoAP to transmit large RGB-D sensor data. In the last section, an outlook of possible improvements and future research will be given.

5.1 Summary

The goal of this thesis was to show that CoAP may function as a lightweight communication protocol to transmit RGB-D sensor data. As a contribution of this thesis, a simple scan application that uses the state of the art Intel RealSense D400 stereo depth sensors and a CoAP resource API have been proposed. Compared to *libcoap*, the application server performs very well in response time but leaves much potential in memory optimizations. The first transmission of a color or a depth packet usually takes longer than following transmissions because the first grab with a cold sensor induces a short delay. Hence a higher variance follows. Experiments 4.1.4 and 4.1.9 have shown that the network overhead becomes a bottleneck, when large data is being transferred with CoAP because of message loss, retransmission timeouts and the nature of stop and wait. With default protocol parameters, a client waits 3 s before it assumes that the first transmission did not reach the server. An interesting approach to speed up transmission times in CoAP would be to set the `NSTART` variable from RFC7252 [5] to a value greater than 1. Using the MQTT protocol data can be transmitted faster due to TCP's sliding window. For example a 10 MB file was transferred in 0.04 s with the *mosquitto_pub* and *mosquitto_sub* applications from the mosquitto MQTT broker, where publisher and subscriber have been running on the desktop computer, listed in Table 3.2. Compared to the results from experiment 4.1.8 where the fastest transmission was 0.42 s, MQTT would be about 9 times faster than CoAP. But effectively, all transmission times, except those measured with *libcoap*, from Section 4.1 include processing delay, i.e. the time it takes to grab an image with the sensor. On constraint devices the TCP sliding window might even be reduced to 1, which makes MQTT fall back to simple stop and wait. Tests have shown that the transmission of a point cloud generally takes longer than the transmission of an image. However, scaling the resolution from 640x480 to 1280x720 does not triple the transmission times because there is a constant processing overhead, including image grab time. For color frames, the higher resolution scales the number of instructions by ca. 1.6 and the number of data references by 1.53. For point cloud the number of instructions is scaled by 2.07 and the number of data referenced becomes scaled by 1.93. Cache miss rates are mostly below 1%. Test case 10, related to test case 9, leads to the conclusion that decimation post processing improves transmission times by ca. 68%. Test cases 5 and 11 show that the application may run on an embedded system, such as the Odroid-Xu4 without suffering from higher response times. Generally, transmission times in a network are very high for full resolution images and point clouds. Thus, the conclusion of this thesis is that CoAP is only conditionally suitable to transmit large point cloud and image data if some point subsampling can be performed and a limited 3D region of interest is known and a low resolution for color images can be use. Despite the fact that CoAP runs over UDP, live streaming with default protocol parameters is not a suitable application for CoAP.

5.2 Future Work

Most significantly, future work includes to make use of a resource directory. The resource directory serves as a central point to discover measurement groups, i.e. multicast groups of CoAP endpoint whose cameras are configured to have a common coordinate system. The resource directory should provide the current number of group members because the client that issues a multicast request to a measurement group must know how many endpoint it can expect a response from. For now the client waits until the multicast response timeout has expired, before computations are done. Secondly, a mechanism to synchronize the point in time when multiple cameras take an image must be found. At the same endpoint one could use sync-cables and across a network a time protocol could be used to coordinate device timers and the recipient should drop a response if it's timestamps drifts away too far.

Bibliography

[1] Statista. *Internet of Things (IoT) connected devices installed base worldwide from 2015 to 2025 (in billions).* 2015. URL: https://www.statista.com/statistics/471264/iot-number-of-connected-devices-worldwide/ (visited on 06/17/2019).

[2] Prasse et al. "New Approaches for Singularization in Logistic Applications Using Low Cost 3D Sensors". In: *Sensing Technology: Current Status and Future Trends IV. Smart Sensors, Measurement and Instrumentation, vol 12. Springer, Cham* (2015).

[3] Luis Barreto, António Amaral, and Teresa Pereira. "Industry 4.0 implications in logistics: an overview". In: *Procedia Manufacturing* 13 (Dec. 2017), pp. 1245–1252.

[4] Andrew Banksm et al. *MQTT Version 5.0.* Tech. rep. OASIS, 2018. URL: http://docs.oasis-open.org/mqtt/mqtt/v5.0/cs02/mqtt-v5.0-cs02.html (visited on 06/17/2019).

[5] Zach Shelby, Klaus Hartke, and Carsten Bormann. *The Constrained Application Protocol (CoAP).* RFC 7252. RFC Editor, June 2014. URL: https://tools.ietf.org/rfc/rfc7252.txt (visited on 06/17/2019).

[6] Hong Linh Truong Andy Stanford-Clark. *MQTT For Sensor Networks (MQTT-SN)Protocol Specification.* Tech. rep. IBM, 2013.

[7] Statista authors. *Anzahl der beförderten Pakete durch die Deutsche Post in Deutschland von 2016 bis 2018 (in Millionen Stück).* URL: https://de.statista.com/statistik/daten/studie/476935/umfrage/anzahl-der-befoerderten-pakete-durch-die-deutsche-post/ (visited on 06/17/2019).

[8] Fielding et al. *Hypertext Transfer Protocol – HTTP/1.1.* RFC 2616. RFC Editor, June 1999. URL: https://tools.ietf.org/rfc/rfc2616.txt (visited on 06/17/2019).

[9] Roy Thomas Fielding. *Architectural Styles and the Design of Network-based Software Architectures.* Tech. rep. UNIVERSITY OF CALIFORNIA, IRVINE, 2000. URL: https://www.ics.uci.edu/~fielding/pubs/dissertation/top.htm (visited on 06/17/2019).

[10] Berners-Lee et al. *Uniform Resource Identifier (URI): Generic Syntax.* RFC 3986. RFC Editor, Jan. 2005. URL: https://tools.ietf.org/rfc/rfc3986.txt (visited on 06/17/2019).

[11] Angelo P. Castellani et al. *Guidelines for Mapping Implementations: HTTP to the Constrained Application Protocol (CoAP).* RFC 8075. RFC Editor, Feb. 2017. URL: https://tools.ietf.org/rfc/rfc8075.txt (visited on 06/17/2019).

[12] Michael Zollhöfer et al. “State of the Art on 3D Reconstruction with RGB-D Cameras”. In: *Computer Graphics Forum* 37 (May 2018), pp. 625–652.

[13] Akbar Rahman and Esko Dijk. *Group Communication for the Constrained Application Protocol (CoAP)*. RFC 7390. RFC Editor, Oct. 2014. URL: `https://tools.ietf.org/rfc/rfc7390.txt` (visited on 06/17/2019).

[14] Zach Shelby et al. *CoRE Resource Directory - draft-ietf-core-resource-directory-20*. Internet-Draft. RFC Editor, Mar. 2019. URL: `https://tools.ietf.org/id/draft-ietf-core-resource-directory-20.txt` (visited on 06/17/2019).

[15] Cenk Gündoğan et al. “NDN, CoAP, and MQTT: A Comparative Measurement Study in the IoT”. In: *Proceedings of ACM ICN 2018* (2018). eprint: `arXiv:1806.01444`.

[16] Muhammad Harith Amaran et al. “A Comparison of Lightweight Communication Protocols in Robotic Applications”. In: *Procedia Computer Science* 76 (Dec. 2015), pp. 400–405.

[17] Dinesh Thangavel et al. “Performance evaluation of MQTT and CoAP via a common middleware”. In: *2014 IEEE Ninth International Conference on Intelligent Sensors, Sensor Networks and Information Processing (ISSNIP)*. IEEE, Apr. 2014. URL: `https://doi.org/10.1109%2Fissnip.2014.6827678` (visited on 06/17/2019).

[18] Carsten Bormann and Zach Shelby. *Block-Wise Transfers in the Constrained Application Protocol (CoAP)*. RFC 7959. RFC Editor, Aug. 2016. URL: `https://tools.ietf.org/rfc/rfc7959.txt` (visited on 06/17/2019).

[19] Klaus Hartke. *Observing Resources in the Constrained Application Protocol (CoAP)*. RFC 7641. RFC Editor, Sept. 2015. URL: `https://tools.ietf.org/rfc/rfc7641.txt` (visited on 06/17/2019).

[20] Badis Djamaa and Ali Yachir. “A Proactive Trickle-based Mechanism for Discovering CoRE Resource Directories”. In: *Procedia Computer Science* 83 (Dec. 2016), pp. 115–122.

[21] Badis Djamaa et al. “Towards efficient distributed service discovery in low-power and lossy networks”. In: *Wireless Networks* 20 (June 2014), pp. 2437–2453.

[22] Markel Iglesias-Urkia, Adrián Orive, and Aitor Urbieta. “Analysis of CoAP Implementations for Industrial Internet of Things: A Survey”. In: *Procedia Computer Science* 109 (2017), pp. 188–195.

[23] Hagen Borstell et al. “Flexible 3D-Smart-Sensoren für Anwendungen in der Logistik und Produktion”. In: Dec. 2016, pp.103–112.

[24] Felix Endres et al. “3D Mapping with an RGB-D Camera”. In: *IEEE TRANSACTIONS ON ROBOTICS* 30 (2014).

[25] S. R. Fanello et al. “HyperDepth: Learning Depth from Structured Light without Matching”. In: *2016 IEEE Conference on Computer Vision and Pattern Recognition (CVPR)*. June 2016, pp. 5441–5450.

[26] Miles Hansard et al. *Time-of-Flight Cameras: Principles, Methods and Applications.* Springer Publishing Company, Incorporated, 2012.

[27] Wasenmüller O.and Stricker D. "A Comparison of Kinect V1 and V2 Depth Images in Terms of Accuracy and Precision". In: *Chen CS., Lu J., Ma KK. (eds) Computer Vision – ACCV 2016 Workshops. ACCV 2016. Lecture Notes in Computer Science, vol 10117. Springer, Cham* (2017).

[28] Intel. *Intel® RealSense™ Depth Camera D400-Series.* Tech. rep. Intel, 2017. URL: `https://www.mouser.com/pdfdocs/Intel_D400_Series_Datasheet.pdf` (visited on 06/17/2019).

[29] Paul Munro and Antony P Gerdelan. "Stereo Vision Computer Depth Perception". In: (May 2019).

[30] Anders Grunnet-Jepsen et al. "Projectors for Intel®RealSense™ Depth Cameras D4xx". In: *Intel Support* (2018). URL: `https://www.intelrealsense.com/wp-content/uploads/2019/03/WhitePaper_on_Projectors_for_RealSense_D4xx_1.0.pdf` (visited on 06/17/2019).

[31] Monica Carfagni et al. "Metrological and Critical Characterization of the Intel D415 Stereo Depth Camera". In: *Sensors* 19 (Jan. 2019), p. 489.

[32] Anders Grunnet-Jepsen, John N. Sweetser, and John Woodfill. "Best-Known-Methods for Tuning Intel® RealSenseTM D400 Depth Cameras for Best Performance". In: *Intel Support* (2018). URL: `https://www.intel.com/content/dam/support/us/en/documents/emerging-technologies/intel-realsense-technology/BKMs_Tuning_RealSense_D4xx_Cam.pdf` (visited on 06/17/2019).

[33] Philip Krejov and Anders Grunnet-Jepsen. "Intel RealSense Depth Camera over Ethernet". In: *Intel Support* (2019). URL: `https://www.intelrealsense.com/wp-content/uploads/2019/03/Depth_Camera_powered_by_Ethernet_WhitePaper.pdf` (visited on 06/17/2019).

[34] Anders Grunnet-Jepsen and Dave Tong. "Depth Post-Processing for Intel® RealSense™ D400 Depth Cameras". In: *Intel Support* (2018). URL: `https://www.intel.com/content/dam/support/us/en/documents/emerging-technologies/intel-realsense-technology/Intel-RealSense-Depth-PostProcess.pdf` (visited on 06/17/2019).

[35] Anders Grunnet-Jepsen et al. "Using the Intel® RealSenseTMDepth cameras D4xx in Multi-Camera Configurations". In: *Intel Support* (2018). URL: `https://www.intel.com/content/dam/support/us/en/documents/emerging-technologies/intel-realsense-technology/RealSense_Multiple_Camera_WhitePaper.pdf` (visited on 06/17/2019).

[36] Intel. *Intel®RealSense™ D400 SeriesCalibrationTools.* Tech. rep. Intel, 2019. URL: `https://www.intel.com/content/dam/support/us/en/documents/emerging-technologies/intel-realsense-technology/RealSense_D400_Dyn_Calib_User_Guide.pdf` (visited on 06/17/2019).

[37] Martin Wegner and Dr. Markus Kückelhaus. "LOW-COST SENSOR TECHNOLOGY A DHL perspective on implications and use cases for the logistics industry". In: *DHL Customer Solutions & Innovation* (2013). URL: `https://delivering-tomorrow.com/wp-content/uploads/2015/08/CSI_Studie_Low_Sensor.pdf` (visited on 06/17/2019).

[38] Rod Deakin. “3-D Coordinate Transformations”. In: 58 (Jan. 1999), pp. 223–34.

[39] Dr. David L. Mills et al. *Network Time Protocol Version 4: Protocol and Algorithms Specification*. RFC 5905. RFC Editor, June 2010. URL: `https://tools.ietf.org/rfc/rfc5905.txt` (visited on 06/17/2019).

[40] Jakub Czyz et al. “Taming the 800 pound gorilla: The rise and decline of NTP DDoS attacks”. In: *Proceedings of the ACM SIGCOMM Internet Measurement Conference, IMC* (Nov. 2014), pp. 435–448.

[41] Zach Shelby. *Constrained RESTful Environments (CoRE) Link Format*. RFC 6690. RFC Editor, Aug. 2012. URL: `https://tools.ietf.org/rfc/rfc6690.txt` (visited on 06/17/2019).

[42] cJSON Developers. *The cJSON Library*. URL: `https://github.com/DaveGamble/cJSON` (visited on 06/17/2019).

[43] RealSense Developers. *The RealSense Library*. URL: `https://github.com/IntelRealSense/librealsense` (visited on 06/17/2019).

[44] Shinji Oomori, Takeshi Nishida, and Shuichi Kurogi. “Point cloud matching using singular value decomposition”. In: *Artificial Life and Robotics* 21 (June 2016), pp. 149–154.

[45] GSL Developers. *The GNU Scientific Library*. URL: `https://www.gnu.org/software/gsl/` (visited on 06/17/2019).

[46] ArUco Developers. *The ArUco Library*. URL: `https://sourceforge.net/projects/aruco/` (visited on 06/17/2019).

[47] RealSense Developers. *GitHub WiKi of RealSense Library*. URL: `https://github.com/IntelRealSense/librealsense/wiki` (visited on 06/17/2019).

[48] Alberto López-Cerón and José M. Cañas. “Accuracy analysis of marker-based 3D visual localization”. In: *Jornadas de Automática* (2016).

[49] OpenCV Developers. *The OpenCV Library*. URL: `https://github.com/opencv/opencv/tree/3.4` (visited on 06/17/2019).

[50] OpenGL Developers. *OpenGL*. URL: `https://www.opengl.org/` (visited on 06/17/2019).

[51] GLEW Developers. *GLEW*. URL: `http://glew.sourceforge.net/` (visited on 06/17/2019).

[52] GLFW Developers. *GLFW*. URL: `https://www.glfw.org/` (visited on 06/17/2019).

[53] glm Developers. *glm*. URL: `https://github.com/g-truc/glm` (visited on 06/17/2019).

Appendix

A.1 JSON format of resource ”/cams/<serial nr.>/depth-settings“

```
{
    "format":"Z16",
    "fps":30,
    "width":1280,
    "height":720
}
```

Listing A.1: Expected payload encoding of resource “/cams/<serial nr.>/depth-settings”

A.2 JSON format of resource ”/cams/<serial nr.>/color-settings“

```
{
    "format":"BGR8",
    "fps":30,
    "width":1280,
    "height":720
}
```

Listing A.2: Expected payload encoding of resource “/cams/<serial nr.>/color-settings”

A.3 JSON format of resource ”/cams/<serial nr.>/application-config“

```
{
  "roi2d":
  {
    "pxx":0,
    "pxy":0,
    "width": 1280,
    "height": 720
  },
  "roi3d":
  {
    "min_x":-0.25,
    "max_x":0.25,
    "min_y":-0.25,
    "max_y":0.25,
    "min_z":0.1,
    "max_z":0.3
  },
    "depth_grab_timeout_ms":10000,
    "color_grab_timeout_ms":10000,
    "icp":1,
    "postprocessing":
    {
        "decimation":1,
        "spatial":1,
        "holefilling":0
    }
}
```

Listing A.3: Expected payload encoding of resource “/cams/<serial nr.>/application-config”

A.4 JSON format of resource "/cams/<serial nr.>/3d-transformation“

```
{
  "scale_matrix" : [[1.000000],[1.000000],[1.000000]],
  "rotation_matrix" : [[0.999524,0.030429,-0.005019],
                       [0.030511,-0.999388,0.017115],
                       [-0.004495,-0.017260,-0.999841]],
  "translation_matrix" : [[-0.113241],[0.111672],[-0.769009]],
  "post_scale_matrix" : [[1.000000],[1.000000],[1.000000]],
  "post_rotation_matrix" : [[0.000000],[0.000000],[0.000000]],
  "post_translation_matrix" : [[0.000000],[0.000000],[0.000000]]
}
```

Listing A.4: Expected payload encoding of resource “/cams/<serial nr.>/3d-transformation”

A.5 JSON format of resource "/cams/<serial nr.>/advanced-config“

```
{
    "aux-param-autoexposure-setpoint": "400",
    "aux-param-colorcorrection1": "0.461914",
    "aux-param-colorcorrection10": "-0.553711",
    "aux-param-colorcorrection11": "-0.553711",
    "aux-param-colorcorrection12": "0.0458984",
    "aux-param-colorcorrection2": "0.540039",
    "aux-param-colorcorrection3": "0.540039",
    "aux-param-colorcorrection4": "0.208008",
    "aux-param-colorcorrection5": "-0.332031",
    "aux-param-colorcorrection6": "-0.212891",
    "aux-param-colorcorrection7": "-0.212891",
    "aux-param-colorcorrection8": "0.68457",
    "aux-param-colorcorrection9": "0.930664",
    "aux-param-depthclampmax": "65536",
    "aux-param-depthclampmin": "0",
    "aux-param-disparityshift": "0",
    "controls-autoexposure-auto": "True",
    "controls-autoexposure-manual": "33000",
    "controls-color-autoexposure-auto": "False",
    "controls-color-autoexposure-manual": "650",
    "controls-color-backlight-compensation": "0",
    "controls-color-brightness": "0",
    "controls-color-contrast": "50",
    "controls-color-gain": "64",
    "controls-color-gamma": "300",
    "controls-color-hue": "0",
    "controls-color-power-line-frequency": "3",
    "controls-color-saturation": "64",
    "controls-color-sharpness": "50",
    "controls-color-white-balance-auto": "True",
    "controls-color-white-balance-manual": "4600",
    "controls-depth-gain": "16",
    "controls-depth-white-balance-auto": "False",
    "controls-laserpower": "150",
    "controls-laserstate": "on",
    "ignoreSAD": "0",
    "param-autoexposure-setpoint": "400",
    "param-censusenablereg-udiameter": "9",
    "param-censusenablereg-vdiameter": "9",
    "param-censususize": "9",
    "param-censusvsize": "9",
    "param-depthclampmax": "65536",
    "param-depthclampmin": "0",
    "param-depthunits": "1000",
    "param-disableraucolor": "0",
    "param-disablesadcolor": "0",
    "param-disablesadnormalize": "0",
    "param-disablesloleftcolor": "0",
    "param-disableslorightcolor": "0",
    "param-disparitymode": "0",
    "param-disparityshift": "0",
    "param-lambdaad": "800",
    "param-lambdacensus": "26",
    "param-leftrightthreshold": "24",
    "param-maxscorethreshb": "2047",
    "param-medianthreshold": "500",
    "param-minscorethresha": "1",
    "param-neighborthresh": "7",
    "param-raumine": "1",
    "param-rauminn": "1",
    "param-rauminnssum": "3",
    "param-raumins": "1",
    "param-rauminw": "1",
    "param-rauminwesum": "3",
    "param-regioncolorthresholdb": "0.0499022",
    "param-regioncolorthresholdg": "0.0499022",
    "param-regioncolorthresholdr": "0.0499022",
    "param-regionshrinku": "3",
    "param-regionshrinkv": "1",
    "param-robbinsmonrodecrement": "10",
    "param-robbinsmonroincrement": "10",
    "param-rsmdiffthreshold": "4",
    "param-rsmrauslodiffthreshold": "1",
    "param-rsmremovethreshold": "0.375",
    "param-scanlineedgetaub": "72",
    "param-scanlineedgetaug": "72",
    "param-scanlineedgetaur": "72",
    "param-scanlinep1": "60",
    "param-scanlinep1onediscon": "105",
    "param-scanlinep1twodiscon": "70",
    "param-scanlinep2": "342",
    "param-scanlinep2onediscon": "190",
    "param-scanlinep2twodiscon": "130",
    "param-secondpeakdelta": "325",
    "param-texturecountthresh": "0",
    "param-texturedifferencethresh": "0",
    "param-usersm": "1",
    "param-zunits": "1000",
    "stream-depth-format": "Z16",
    "stream-fps": "30",
    "stream-height": "720",
    "stream-width": "1280"
}
```

Listing A.5: Expected payload encoding of resource “/cams/<serial nr.>/advanced-config”

I herewith assure that I wrote the present thesis titled *3D Scan Applications in Logistics: Using CoAP with RGB-D Cameras* independently, that the thesis has not been partially or fully submitted as graded academic work and that I have used no other means than the ones indicated. I have indicated all parts of the work in which sources are used according to their wording or to their meaning.

I am aware of the fact that violations of copyright can lead to injunctive relief and claims for damages of the author as well as a penalty by the law enforcement agency.

Magdeburg, August 6, 2020

(Fabian Hüßler)